A remote sensing data fusion method for continuous daily evapotranspiration mapping at kilometric scale in Sahelian areas

Aubin Allies, Albert Olioso, Bernard Cappelaere, Gilles Boulet, Jordi Etchanchu, Hélène Barral, Ibrahim Bouzou Moussa, Jean-Philippe Chazarin, Emilie Delogu, Hassane Bil-Assanou Issoufou, et al.

Version of Record: https://www.sciencedirect.com/science/article/pii/S0022169422000798
Manuscript_effb321b1fa574441e791c2e7e5f51fd

A remote sensing data fusion method for continuous daily evapotranspiration mapping at kilometric scale in Sahelian areas

[1]Aubin Allies[a], Albert Olioso[b], Bernard Cappelaere[a], Gilles Boulet[c], Jordi Etchanchu[a], Hélène Barral[a], Ibrahim Bouzou Moussa[d], Jean-Philippe Chazarin[a], Emilie Delogu[c], Hassane Bil-Assanou Issoufou[e], Ibrahim Mainassara[a,f], Monique Oï[a], Jérôme Demarty[a]

[a]HydroSciences Montpellier (HSM), Univ Montpellier, CNRS, IRD, 300 avenue du Professeur Emile Jeanbrau, 34090 Montpellier, France; allies.aubin@orange.fr (A.A.); bernard.cappelaere@ird.fr (B.C.); helene.barral@umontpellier.fr (H.B.); jean-philippe.chazarin@ird.fr (J-P. C.); jordi.etchanchu@ird.fr (J.E.); ibrahim.mainassara@ird.fr (I.M.); monique.oi@ird.fr (M.O.); jerome.demarty@ird.fr (J.D.)

[b]Environnement Méditerranéen et Modélisation des AgroHydrosystèmes (EMMAH), INRAE, Avignon Université, 228 route de l'Aérodrome Domaine Saint Paul – Site Agroparc, 84914 Avignon, France; now at Unité de Recherche écologie des Forêts Méditerranéennes (URFM), INRAE, Avignon ; albert.olioso@inrae.fr

[c]Centre d'Etudes Spatiales de la BIOsphère (CESBIO), Université de Toulouse, CNRS, CNES, IRD, UPS, INRAE, 18 avenue Édouard Belin, 31400 Toulouse, France; gilles.boulet@ird.fr (G.B.); delogue@cesbio.cnes.fr (E.D.)

[d]Université Abdou Moumouni, Niamey, Niger; ibrahimbm1958@gmail.com

[e]Department of Crop Science and Technology, Université Dan Dicko Dankoulodo de Maradi, Maradi, Niger; hassanebil-assanou.issoufou@ird.fr

[f]Institut de Recherche pour le Développement (IRD) Representation, 276 avenue de Maradi, Niamey, Niger

Correspondence: aubin.allies@orange.fr

Abstract: Thermal infrared (TIR) remote sensing-based ET estimates are very appealing for a wide range of scientific applications in hydrology. However, they are prone to infrequency due to satellite revisit interval and cloud cover. Temporal interpolation techniques or multi-resolution and multi-frequency data fusion approach have thus recently been studied to provide continuous ET estimates. It has been already shown that the interest of temporal interpolation techniques is limited to short return interval that is troublesome in Sahelian regions where mesoscale convective systems linked to the West African Monsoon (WAM) renders unusable most of TIR images during the rainy season. Here we developed a data fusion approach to provide remote sensing-based continuous daily ET estimates at kilometric resolution in Sahelian areas. The proposed algorithm fill gaps in MODIS-based ET estimates from EVASPA S-SEBI Sahel (E3S) using the Global Land Evaporation: the Amsterdam Methodology (GLEAM) product and/or ET estimates from a simple parametric model for typical Sahelian ecosystems as a normalized basis. The fusion algorithm is evaluated at the

[1] Present affiliation:
GEOSYS B Park – Bâtiment B, 2 rue Joseph Hubert 31130 Balma, France

pixel scale against eddy-covariance measurements and simulations of a locally calibrated and validated land surface model (LSM) on a millet crop and a fallow of shrubby savannah in the southwest of the Republic of Niger. Consistency of the fusion approach is also evaluated at mesoscale by comparing it with a set of 20 regional LSMs. Globally both level of comparison highlight the very good agreement of ET estimates based on the fusion approach with both in situ measurements and LSMs simulations. We also show the benefit of such a fusion approach compared to linear temporal interpolation techniques of the ratio between ET and either incoming solar radiation or reference evapotranspiration. The main benefits are observed during the first months of the rainy season in the depiction of the surface response to rainfall events and consecutive drying up of the surface soil layer. We suggest that such a fusion approach could be later used in disaggregation chain to enhance field scaled ET estimates by the combination of coarse, moderate and high resolution remote sensing-based ET estimates.

Keywords: evapotranspiration, data fusion, E3S, GLEAM, MODIS, Sahel

1. Introduction

Evapotranspiration (ET) is a key variable in the coupled water and energy cycles. It is involved in numerous biophysical and biochemical process (Katul et al., 2012). Its estimation in space and time is thus crucial for a wide range of scientific and operational applications (Fisher et al., 2017), including: understanding and forecasting global change in water (Jung et al., 2010; Marshall et al., 2012), managing irrigation (Santos et al., 2007; Toureiro et al., 2017), managing and forecasting severe drought events (Anderson et al., 2016, 2010; Otkin et al., 2016), regional water balance and groundwater monitoring (Olioso et al., 2018, 2015; Ollivier et al., 2021; Ruggieri et al., 2021), or constraining and calibrating distributed hydrological models (Kunnath-Poovakka et al., 2016; Schuurmans et al., 2003; Tobin and Bennett, 2017). As it is controlled by several biotic and abiotic factors, ET is highly variable spatially (Alfieri et al., 2007). However, in-situ measurements acquired for example using lysimeters, eddy correlation systems or scintillometers, are only able to provide estimates at small scales (10^0-10^3 m). These measurements still are essential for model calibration and validation and for biophysical process monitoring at fine spatiotemporal scale (Boulain et al., 2009b; Ramier et al., 2009; Velluet et al., 2014), although they cannot fulfill the need for ET estimates at regional to continental scales.

In this respect, remote sensing (RS) -based approaches are promising (Zhang et al., 2016) especially for the African continent where field measurements are scarce. In particular, the response of land surface temperature (LST) to the intensity of water stress through the surface energy balance makes this variable a key target for estimating ET from space (Kalma et al., 2008). Nevertheless, estimation of ET from thermal infrared (TIR) data still has limitations. The main one is the intermittency of image acquisition at moderate and high resolutions, which hinders the feasibility of continuous monitoring of ET. Intermittent acquisition is due both to the revisit frequency of the satellite which is governed by its orbital configuration and to cloud cover occurrence (Alfieri et al., 2017; Guillevic et al., 2019; Lagouarde et al., 2013). This last point is particularly critical in West Africa where climate is governed by a monsoon regime characterized by mesoscale convective systems that make many of the TIR images

acquired during the rainy season not usable. Allies et al. (2020) showed that despite having a daily return interval, MODIS TIR images availability did not exceed 6 images per month on average during the rainy season in four years of data over South West Niger. Little studies have so far focused on the reconstruction of ET between two dates with suitable acquisition. In most cases, a simple linear interpolation of the ratio between ET and a known reference quantity is performed (Alfieri et al., 2017; Delogu et al., 2021; Guillevic et al., 2019; Lagouarde et al., 2010). This quantity can be the incoming solar radiation (Gallego-Elvira et al., 2013), the extra-terrestrial solar radiation (Guillevic et al., 2019; Ryu et al., 2012), or the reference evapotranspiration (ET_0) (Cammalleri et al., 2013). Other interpolation methods were proposed (e.g. cubic and Hermite spline) but proved to be less reliable than the linear method (Alfieri et al., 2017). The interpolation supports should carry information on variations in the drivers of ET between two acquisition dates. ET drivers are essentially related to available energy or to water availability (available water for plants and soil evaporation). Most supports commonly used so far provide information only on energy constraints in relation to solar radiation or on atmospheric water demand in the case of ET_0. Linear interpolation based on ET_0 or Rg cannot account for variations in ET related to other drivers than Rg or ET_0. Among unaccounted-for effects are, e.g., (i) the impact of re-humectations related to water supplies occurring between acquisition days, (ii) the evolution of vegetation cover, (iii) the non-linearity of the drying kinetic of soil top layers and (iv) the non-linear responses of stomatal conductance to soil moisture and atmospheric demand. This is all the more important as the time between two successive available ET data is long. Alfieri et al. (2017) and Delogu et al. (2021) showed that the interest of these basic temporal interpolation schemes was limited to short return intervals of less than 8 days. In order to improve interpolation, it may be possible to use variables that more closely follow ET variations. It is not required that these estimations are fully accurate, but they need to respond to more ET drivers than only Rg or ET_0, and in particular to precipitation and drying kinetics. Delogu et al. (2021) showed that the inclusion of additional information related to the timing of rainfall events may help in improving the monitoring of daily ET. This is particularly true in the Sahel where soil drainage is fast and the response of surface is abrupt after each rainfall event (Lohou et al., 2014).

Considering the limitations of temporal interpolation schemes, techniques of multiple data source fusion are attractive as they take advantage of information provided by several datasets (Cammalleri et al., 2013; Gao et al., 2006; Li et al., 2017). The use of multi-resolution ET products is interesting to fill gaps in moderately or highly spatially-resolved products with temporal information contained in coarser ones. For instance, Cammalleri et al. (2013) adapted the Spatial and Temporal Adaptive Reflectance Fusion Model (STARFM), which was originally developed for generating “a synthetic daily surface reflectance product at Landsat Enhanced Thematic Mapper Plus (ETM+) spatial resolution” by Gao et al. (2006), to produce continuous “Landsat-like” daily ET images using temporal series of MODIS images. STARFM was later applied and evaluated in various eco-climatic conditions (Cammalleri et al., 2014; Gevaert and García-Haro, 2015; Semmens et al., 2016; Wang et al., 2014). Other algorithms have been proposed to produce fine scale ET maps from Landsat-MODIS data fusion algorithms based on upstream LST disaggregation (Eswar et al., 2016; Olivera-Guerra

et al., 2017; Zhang et al., 2021), simple linear regression (Bhattarai et al., 2015) or machine learning (Ke et al., 2017). Nonetheless if such data fusion techniques are engaging to produce field scale ET estimates, they are prone to MODIS data gaps due to cloud cover and data quality, restricting the reconstruction of daily ET maps. Thus, in order to reconstruct continuous daily ET time series, MODIS ET estimates need to be temporally interpolated in a first step. Generally, linear interpolation of an ET-reference quantity ratio were used (Cammalleri et al., 2013; Ma et al., 2018). A similar interpolation scheme was used by Gallego-Elvira et al. (2013) and Olioso et al. (2018) to reconstruct sequences of daily ET from MODIS data. As MODIS data are coming with a daily revisit, one may think that such a simple interpolation procedure is sufficient. However, in many situations, as the monsoon season in Sahelian regions for example, the cloud occurrence can significantly increase and drastically reduce the number of available ET estimates (Allies et al., 2020). The fusion of MODIS estimates with other information having a daily time step (or finer) can be proposed for improving the production of continuous ET estimates. It might be possible to use information such as surface variables in weather forecast model reanalysis, simulations of distributed water balance model fed by remote sensing data (e.g. GLEAM, Miralles et al., 2011) or results from Land Data Assimilation Systems (e.g. Albergel et al., 2017).

The objective of the present study is to evaluate the capability of a new approach using multiple ET data sources to fill gaps between daily ET maps generated with remote sensing techniques. It is based on a new fusion methodology that makes it possible to derive continuous daily evapotranspiration maps at 1 km resolution by combining intermittent ET estimates from MODIS data to continuous ET monitoring obtained at 0.25° resolution from the GLEAM product. This method uses ET interpolation supports that account for rainy events and drying kinetics both at mesoscale, thanks to the GLEAM data, and at the kilometer scale, thanks to a developed simple ET parametric model named PAMEAS (PArametric Model for Evapotranspiration in the Agropastoral Sahel). In our work, the high-resolution ET maps were produced using the EVASPA S-SEBI Sahel (E3S) approach from MODIS TIR and albedo data, which has shown very good performances over South West Niger (Allies et al., 2020). However, the proposed methodology could be used with any ET mapping and daily mesoscale estimation of ET together with a surface water balance model. The benefits of the data fusion approach were evaluated against standard interpolation schemes. To do so, ET estimates from either the fusion approach or the interpolation schemes were evaluated at field scale against in situ observation acquired on two typical ecosystems of the agropastoral Sahel and at mesoscale against ensemble simulations with Land Surface Models (LSMs). This region is characterized by long periods without usable remote sensing optical data due to heavy cloud cover during the rainy season. To our knowledge this study is the first to deal with the complex issue of the continuous estimation of daily evapotranspiration from TIR images in the Sahel, potentially giving useful information for worldwide areas with long periods of cloudiness.

This paper is structured as follows: materials and methods are introduced in section 2. The study area is firstly presented (section 2.1) followed by the data sets used in fusion and interpolation approaches (section 2.2) and the data sets used for the evaluation of the fusion

and interpolation schemes (section 2.3). The methodology employed is then detailed in section 2.4. Results are presented in section 3 and discussed in section 4. A general conclusion is finally given in section 5.

2. Materials and Methods

The fusion method was applied on 4 years (2005-2008) of data at mesoscale in South West Niger, where surface flux observations were collected by the AMMA-CATCH National Observation Service (NOS) (Galle et al., 2018) at two micrometeorological flux towers in a millet crop and a fallow of shrubby savannah, the two main land cover types in the region (Cappelaere et al., 2009). The accuracy of daily evapotranspiration retrievals using E3S was previously evaluated at the same site over the 2005-2008 period (Allies et al., 2020). In the present study, the data fusion approach is evaluated at field scale against in situ surface energy balance measurements (Ramier et al., 2009; Velluet et al., 2014) and simulations with a physically based/calibrated/validated Land Surface Model (LSM), named SiSPAT (Simple Soil-Plant-Atmosphere Transfers, Velluet et al., 2014). It is also evaluated at mesoscale by comparison with the simulations from a set of 20 spatially distributed LSMs selected in the framework of the ALMIP2 intercomparison exercise (Boone et al., 2009; Grippa et al., 2017).

2.1. Study area

The study area is located in the southwest of the Republic of Niger (Figure 1.a). It consists of a mesoscale window (1.55° - 3.15°E; 12.85 - 14.15°N) covering an area of 20 800 km² included in the AMMA-CATCH NOS. It is located in the agropastoral Sahel characterized by a tropical semiarid climate with rainfall ranging from 570 mm to 470 mm along a South-North gradient and with mean temperature of ~ 30 °C (Cappelaere et al., 2009). Climate is governed by the West African Monsoon (WAM), with a long dry season from November to April followed by a rainy season characterized by mesoscale convective systems. The study area is approximately centered on Niger's capital city of Niamey and it is crossed both by the Niger River (western part) and by the Dallol Bosso fossil river valley (eastern part, see Figure 1.b). The main ecosystems of the area are typical of the agropastoral Sahel, alternating between rainfed millet crop and fallow of shrubby savannah (Cappelaere et al., 2009; Leblanc et al., 2008) (Figure 1.b). Remains of tiger bush are also observed, especially over plateau areas. Irrigated orchards and gardens are scattered along the Niger River nearby urban areas in particular in the outskirts of Niamey. Regarding soils and hydrology, the northern and the eastern parts of the study area are characterized by endoreic catchments with sandy soils, weakly structured with sand fraction superior to ~ 75 % and even above 85 % in the Niger River and Dallol Bosso valleys. The latter is characterized by intermittent seasonal flow and pounding during the rainy season and often maintaining subsurface water the rest of the year (Leduc et al., 1997). The right bank of the Niger River is characterized by loamier soils and is less prone to surface crusting. The two main reference plots of the AMMA CATCH Niger mesosite are located in between the two above alluvial valleys, near the Wankama village, at about 60 km northeast of Niamey (2.6°E, 13.6°N; Figure 1.c). These two plots of ~15 ha each have been intensively instrumented since 2005 (Cappelaere et al., 2009). The monitored ecosystems are the two dominant ecosystems in the study area: a pearl millet crop

(*Pennisetum glaucum* (L.) R. Br.) and a fallow composed of patches of a shrub layer dominated by *Guiera senegalensis* Lam., annual C3 and C4 grasslands and bare soils (Boulain et al., 2009a; Ramier et al., 2009). No alternation between millet crop and fallow was observed during the studied ground measurements period (2005-2008). Data acquired in the plots are described in the next Section 2.3.1.

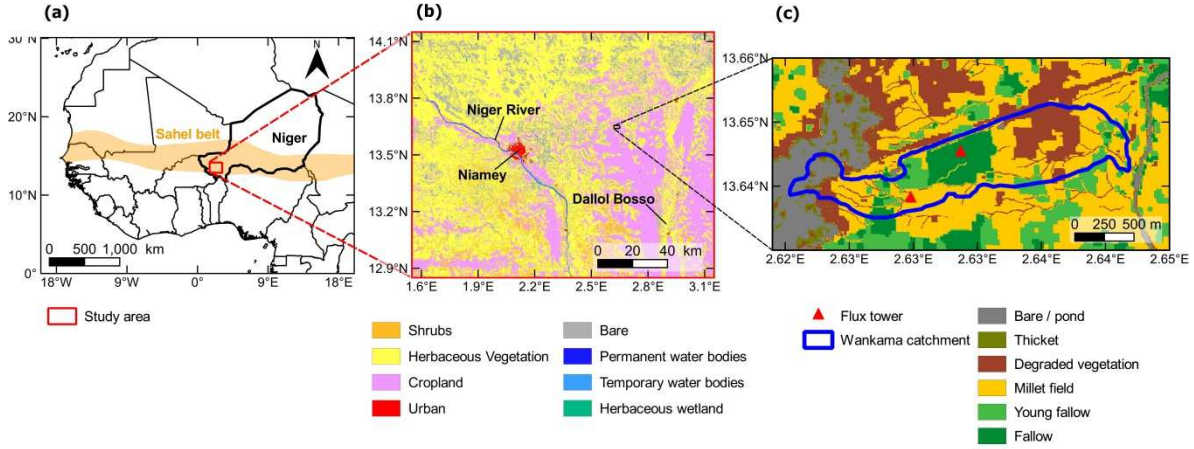

Figure 1. Location of the study mesosite in West Africa (a); Land cover (Copernicus Global Land Service product) (b) and local-scale Wankama catchment with the location of the EC flux towers and land cover map derived from a 2005 SPOT image (c).

2.2. Data sets used in fusion and interpolation approaches

2.2.1. E3S

E3S (EVASPA S-SEBI Sahel) is a contextual RS-based method for daily ET mapping designed to minimize the use of ancillary meteorological data and provide comprehensive epistemic uncertainty of daily ET retrievals for Sahelian areas (Allies et al., 2020). It is based on the EVapotranspiration Assessment from SPAce (EVASPA) RS-based modelling tool (Gallego-Elvira et al., 2013) and the Simplified Surface Energy Balance Index (S-SEBI) method (Roerink et al., 2000). S-SEBI derives ET from the evaporative fraction (EF) computed from surface temperature (LST) and surface albedo (α) of a given satellite scene as follows:

$$EF(LST, \alpha_i) = \frac{LST_{dry}(\alpha_i) - LST_i}{LST_{dry}(\alpha_i) - LST_{wet}(\alpha_i)} \quad (1)$$

where subscript i correspond to a given pixel of a the satellite scene associated with an α_i albedo value and a LST_i surface temperature value. LST_{dry} and LST_{wet} correspond to fully dry (EF = 0) and fully wet (EF = 1) areas respectively, between which EF is assumed to vary linearly (Figure 2).

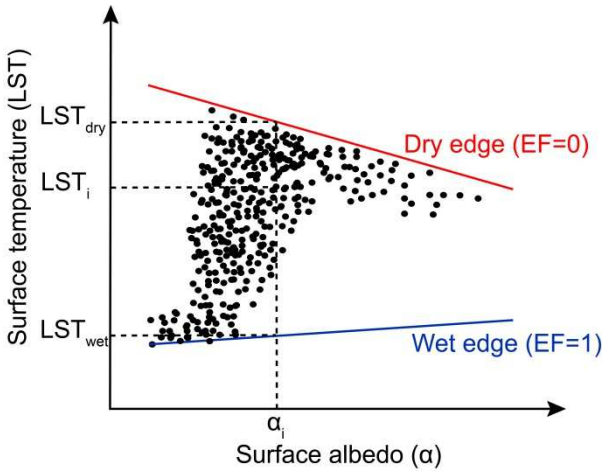

Figure 2. Representation of the relationship between surface albedo, surface temperature, and evaporative fraction according the S-SEBI method (adapted from Allies et al., 2020 and Roerink et al., 2000)

Comparatively to S-SEBI, E3S computes at each satellite overpass time the evaporative fraction by considering 17 methods for the determination of the edges of the LST-α shape. ET derived using the different edges determination methods were averaged to provide an ensemble mean of ET. The average procedure of the 17 ET estimates considered weighting coefficients that were derived according to the seasonal stage of rainfall and LAI (see Allies et al., 2020 for details). The variability of ET estimates was also used to derive an estimation of uncertainty in the derivation of ET. In this work, we use daily ET from 2005 to 2008 derived from E3S using LST and surface albedo from MODIS onboard TERRA and AQUA, as well as incoming longwave and shortwave radiations from flux towers measurements as described by Allies et al. (2020). E3S was already evaluated at the time of satellite overpass and at the daily scale against the data from the two eddy-covariance towers (before gap-filling) and against the SiSPAT simulations by Allies et al. (2020). In average, length of gaps in MODIS-based E3S ET estimates are about 10.3 ±13.5 days and are mainly due to cloud contamination.

2.2.2. GLEAM

GLEAM (Global Land Evaporation: the Amsterdam Methodology) is a global daily ET product at a 0.25° resolution. It is developed by the VU University of Amsterdam (Miralles et al., 2011) and it is designed to maximize the use of satellite-derived observations in combination to climatic re-analysis data. GLEAM derives ET at each grid cell using a Priesley-Taylor model for computing potential evapotranspiration and several stress factors for reducing this potential evapotranspiration. Stress factors depend on the vegetation moisture derived from microwave emission measurements and on soil moisture simulated by a 3 layers soil module. Microwave information is also used for correcting the soil module through a simple data assimilation procedure. The version of the product used in this work is the v3.1.a (Martens et al., 2017). It is forced with radiation fluxes and atmospheric temperature from ERA-Interim (Dee et al., 2011), precipitations from the Multi-Source Weighted Ensemble Precipitation dataset (MSWEP) (Beck et al., 2017) and microwave

surface soil moisture from the ESA Climate Change Initiative soil moisture (ESA CCI SM v2.3) data set (Liu et al., 2012; Wagner et al., 2012). The version 3.1.a of GLEAM has been recently validated against measurements from 91 eddy-covariance towers and 2325 soil moisture sensors (Martens et al., 2017).

2.2.3. PAMEAS

2.2.3.1. Description of the model

PAMEAS (PArametric Model for Evapotranspiration in the Agropastoral Sahel) is a simple parametric model developed in the framework of this study to derive ET from incoming solar radiation (*Rg*), rainfall (*R*) and Leaf Area Index (*LAI*) only, for typical Sahelian ecosystems. PAMEAS computes separately soil evaporation (*E*) and vegetation transpiration (*T*), both as a multiplicative function of *Rg* (Xu and Singh, 2000).

T (mm.day^{-1}) is simulated under no-stressed conditions as a simple function of *Rg*:

$$T = \rho_2 f_{COVER} \frac{Rg}{\lambda} \quad (2)$$

where ρ_2 (-) is a calibrated parameter, λ the latent heat of vaporization (~ 28.4 W.m^{-2}) and f_{COVER} the fraction of vegetation cover.

PAMEAS assumes that the vegetation is not facing water stress. In other words PAMEAS only provides a potential transpiration. Temporal variations of *T* are thus only due to incident solar radiation fluctuations, resistance terms being negligible. f_{COVER} is derived from LAI according a Beer-Lambert law:

$$f_{COVER} = 1 - e^{-0.5\mathrm{LAI}} \quad (3)$$

For soil evaporation *E* (mm.day^{-1}), PAMEAS accounts for the fraction cover by considering the uncovered soil fraction (1-f_{COVER}) and for a stress function depending on the soil water content as approximated by the Antecedent Precipitation Index (API) (Kohler and Linsley, 1951):

$$E = \rho_1 (1 - f_{COVER}) \frac{Rg}{\lambda} \cos\left(\frac{\pi}{2} \frac{SWC_{FC} - API}{SWC_{FC}}\right) \quad (4)$$

with *Rg* (W.m^{-2}) the incoming solar radiation, λ the latent heat of vaporization (~ 28.4 W.m^{-2} for 1 mm.day-1), SWC_{FC} (mm) the soil water content of the surface layer (defined as 0-10 cm) at field capacity, *API* (mm) the calibrated antecedent precipitation index, and ρ_1 (-) a calibrated parameter. The $\pi/2$ term ensures the normalization of the stress factor between 0 (stressed) and 1 (not stressed). A cosine function is used to describe a non-linear evolution of the water stress with the decrease of the surface soil layer water content as proposed by Merlin et al. (2016, 2010) (Figure 3).

The soil water content at field capacity is derived from the sand and clay fraction according to (Saxton et al., 1986):

$$SWC_{FC} = 100\left(\frac{1}{3A}\right)^{\frac{1}{B}} \quad (5)$$

$$A = e^{-4.396-7.15\times10^{-2}f_{clay}-4.88\times10^{-4}f_{sand}^2} \quad (6)$$

$$B = 3.14 - 2.22\times10^{-3}f_{clay}^2 - 3.484\times10^{-5}f_{sand}^2 f_{clay} \quad (7)$$

where f_{clay} and f_{sand} are the soil fraction of clay and sand respectively.

API is computed according the following formulation:

$$API_d = API_{d-1}e^{-\frac{1}{\omega_1}} + \omega_2 R_d \quad (8)$$

with the subscript d for the considered day, ω_1 et ω_2 parameters calibrated on field measurements of the 0-10 cm soil water content, and R (mm) daily rainfall.

Finally PAMEAS computes ET from the sum of soil evaporation (E) and canopy transpiration (T).

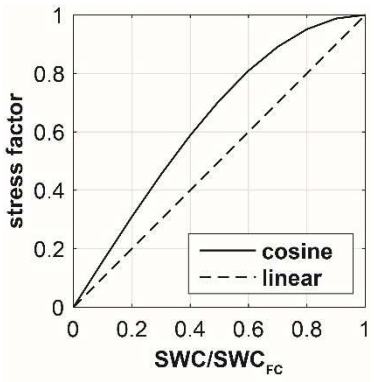

Figure 3. Evolution of the stress factor with the surface soil water content.

Appendix C describes the calibration of the PAMEAS model against SiSPAT simulations at field scale over the 2005-2012 period. SiSPAT model was used to develop and calibrate PAMEAS at field scale because it allows to separate soil evaporation from canopy transpiration.

2.2.3.2. Spatial distribution of the model

PAMEAS was spatialized using sand and clay fractions from ECOCLIMAP2 (Kaptué Tchuenté et al., 2011), precipitation fields derived from rain gauge data over the observational network using Krigged-Lagrangian spatial interpolation method as for ALMIP2 LSMs (Vischel et al., 2011), LAI from MODIS data (MCD15A3 product) and incoming solar radiation from flux towers measurements considering that spatial variations were negligible over the study site (Allies et al., 2020). Rainfall and radiation fields were given at daily timescale. MODIS LAI product was a 4-days composite that was previously interpolated using a cubic spline function. PAMEAS simulations were finally released at the same resolution as MODIS (~1 km).

Two versions of PAMEAS were considered:

- In the first one, PAMEAS parameters (ρ_1, ρ_2, ω_1, ω_2) were simultaneously calibrated on ET time series derived with E3S over the 2005-2008 period for each pixel. To this end, about 104 800 simulations were performed with PAMEAS considering a priori parameters intervals; the best parameter set for each pixel was selected considering minimal Root Mean Square Error (RMSE)
- Alternately, in the second PAMEAS version, only ρ_1 and ρ_2 were calibrated against E3S ET maps. API parameters (ω_1, ω_2) were calibrated on soil moisture simulated by SiSPAT at both flux tower sites (see Appendix C) and they were considered as uniforms over the whole mesoscale study site. API fields were generated for both cover types (millet and fallow) and then averaged to generate a single value to use in PAMEAS. This simplification allowed a strong reduction in the number of simulations and consequently in computing time. As only the two flux tower sites were used for calibrating API parameters, we expect that the spatial representativeness of soil evaporation simulated by PAMEAS will be affected. Conversely, we expect that this version will make it possible to evaluate PAMEAS performance in more details at local scale. Calculation made with this second PAMEAS version were named by adding the subscript "LC", for local calibration, to the fusion method name (e.g. EGP_{LC}).

2.2.4. Incoming solar radiation (Rg) and reference evapotranspiration (ET_0) fields

The developed fusion algorithm is compared to standard temporal interpolation techniques based on the linear interpolation of the ratio between ET and Rg or ET_0. To this end, Rg fields were generated using the average between measurements from both millet and fallow EC stations considering that spatial variations were negligible over the study site. Similarly, ET_0 was computed as in Allen et al. (1998) using Rg, air temperature, air relative humidity and wind speed from the average of millet and fallow plots measurements:

$$\mathrm{ET_0} = \frac{0.408\Delta Rn + \gamma \frac{900}{T_{mean}+273} u_{2m}(e_s - e_a)}{\Delta + \gamma(1 + 0.34u_{2m})} \quad (9)$$

where Rn ($MJ.m^{-2}.day^{-1}$) is the net radiation, T_{mean} (°C) is the mean daily air temperature, u_{2m} ($m.s^{-1}$) is the wind speed at 2 m height, e_s (kPa) is the saturation vapour pressure, e_a (kPa) is the actual vapour pressure (e_a), Δ ($kPa.°C^{-1}$) is the slope of vapour pressure curve and γ ($kPa.°C^{-1}$) is the psychrometric constant.

2.3. Evaluation data sets

2.3.1. Eddy-covariance measurements

The two reference local plots of the AMMA CATCH NOS were equipped for continuous monitoring of meteorological variables (rainfall, air pressure, temperature and humidity, wind

speed and direction, four-component radiations) and soil variables (shallow ground heat flux, temperature and moisture profiles down to a depth of 2.5 m). Eddy Covariance (EC) systems were also implemented, measuring high frequency (20Hz) wind speed (3 components), air temperature and water vapor, to derive sensible and latent heat flux estimates (see Table 1). Turbulent fluxes were derived as described by Ramier et al. (2009), using EdiRe software (R. Clement, University of Edinburgh) and following CarboEurope recommendations (Mauder and Foken, 2004). Full details of the setup and the sensors can be found in Ramier et al., (2009) and Velluet et al. (2014). Several studies already exploited the data acquired or derived from these plots (Boulain et al., 2009b; Lohou et al., 2014; Marshall et al., 2013; Ramier et al., 2009; Sjöström et al., 2013; Velluet et al., 2014). In our study, for purpose of comparison with RS-based daily ET estimates, gaps in eddy covariance-based latent heat flux measurements were filled according to the climatological method proposed by Velluet (2014) (see Appendix A). Only days with less than one third of the data being gap-filled were used in this study. On the overall studied period only 3.5 % and 4.3% of 30-min latent heat measurements were gap-filled with this method for the millet crop and the fallow respectively. After this gap-filling step, the energy balance at the daily scale revealed a slight imbalance of 0.7 $W.m^{-2}$ and 13.8 $W.m^{-2}$ for the millet crop and the fallow respectively. After gap-filling, we disposed of 1149 days of observation, 312 days being missing.

Table 1. Main observations used from the South-West Niger AMMA-CATCH eddy covariance-stations

Instrument	Main measurements	Height or depth
Campbell CSAT-3 sonic anemometer (Campbell Scientific, Inc, Logan, USA	3-D wind Sonic air temperature	5 m (both plots)
LI-COR LI-7500 infrared gas analyser (LI-COR Biosciences, Lincoln, USA)	CO_2 and H_2O concentrations	5 m (both plots)
Kipp&Zonen CNR1 radiometer (Kipp&Zonen, Delft, the Netherlands)	Shortwave (0.3–2.8 µm) and longwave (5–50 µm) incoming and outgoing radiation	3.5 m (Wankama fallow) 2.5 m (Wankama millet)
Hukseflux HFP01SC heat flux plates (3 averaged) (Hukseflux, Delft, the Netherlands)	Soil heat flux	- 0.05 m (both plots)

2.3.2. SiSPAT simulations

The Simple Soil-Plant-Atmosphere Transfers (SiSPAT) model is a physical based LSM able to simulate the coupled heat and water exchanges at the soil-plant-atmosphere interface (Braud et al., 1995). Both energy budgets from the vegetation canopy and the soil surface are solved using a classical electrical analogy in a two-layer system. The SiSPAT model was previously thoroughly calibrated and validated by Velluet et al. (2014) for the 7-years period 2005-2012 against the energy balance and the soil moisture data acquired on the millet crop site and the fallow of shrubby savannah site. Model skill scores against observed half-hourly energy balance components can be found in Velluet et al. (2014) and Allies et al. (2020). Globally scores were very good for both ecosystems (RMSE < 30 Wm^{-2} for millet and RMSE < 40 Wm^{-2} for fallow) considering uncertainty relative to such observations. This suggests that SiSPAT simulations may be considered as reliable proxies of the local plots fluxes with the benefit of no gaps allowing more complete evaluation at pixel scale. Note that SiSPAT simulations were already used to evaluate non-interpolated E3S ET estimates in South-West Niger (Allies et al., 2020).

2.3.3. ALMIP2 Land Surface Model simulations

The AMMA Land surface Model Intercomparaison Project Phase 2 (ALMIP2) (Boone et al., 2009) is dedicated to identify current weaknesses in LSMs representation of surface land processes among 20 models at local and mesoscale in West Africa. Models simulations were

performed at 30 min timescale on the mesoscale site with a 0.05° grid during the 2005-2008 period. The 20 ALMIP2 models are listed in Appendix A. All models were forced with precipitation fields derived from rain gauge data over the observational network using Krigged-Lagrangian spatial interpolation method (Vischel et al., 2011). Incoming longwave and shortwave radiations came from the Satellite Application Facility for Land Surface Analysis (Land-SAF) project (Trigo et al., 2011) whereas all other meteorological forcing variables including air temperature, near surface specific humidity, wind speed and surface atmospheric pressure came from ECMWF ERA-interim re-analysis (Dee et al., 2011). Most of the models used the ECOCLIMAP2 Africa database (Kaptué Tchuenté et al., 2011) to derive soil and vegetation characteristics including LAI. Nevertheless some of them had their own formulations or specific data for some variables (see Grippa et al., 2017 for more details). In this study, we used the ensemble average and standard deviation of LSMs simulations in term of spatial mean over our study site as a basis of comparison at mesoscale.

2.4. Methodology

The methodology used is exposed in Figure 4 and detailed in the following subsections.

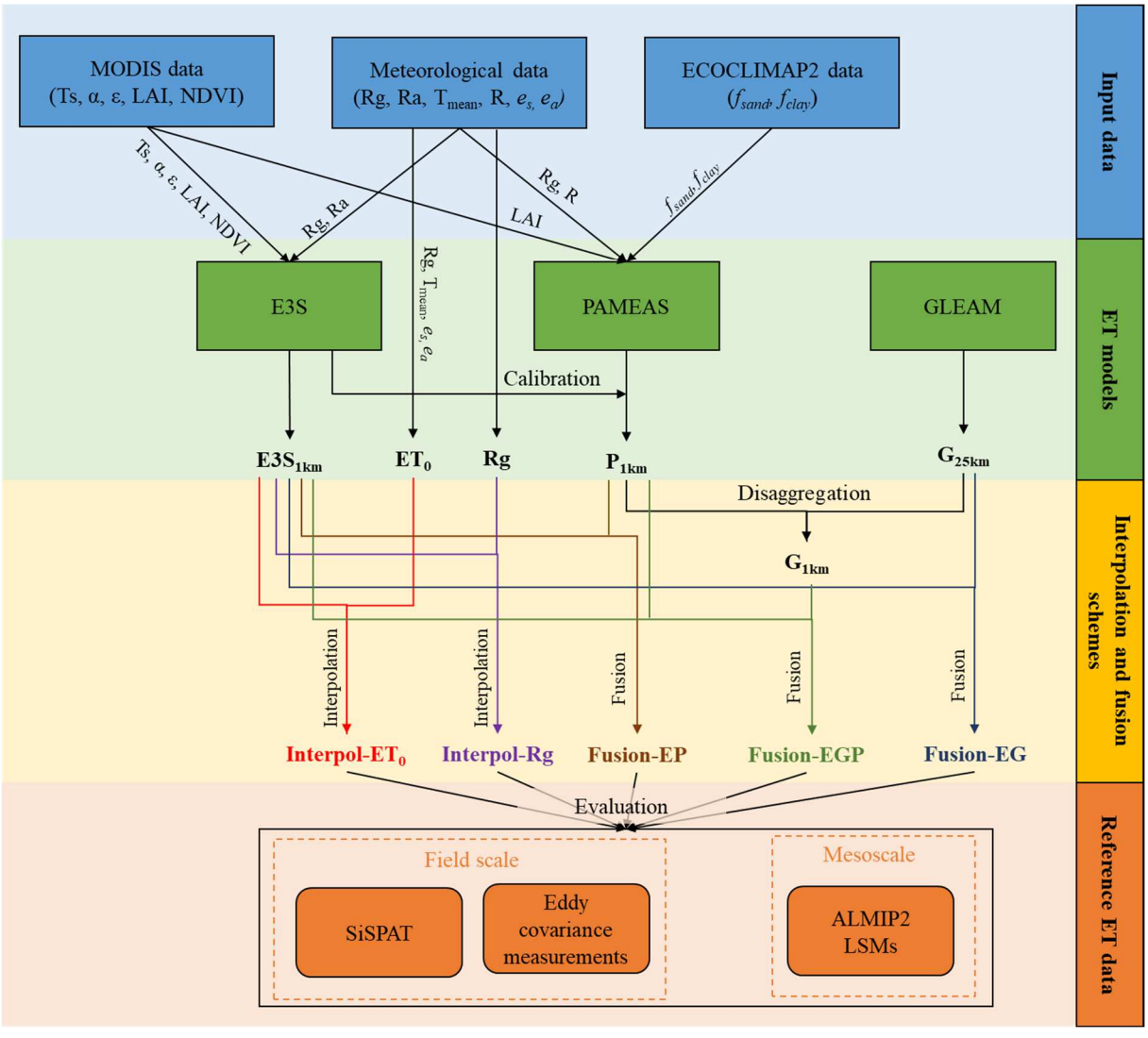

Figure 4. Flowchart of the methodology employed for the generation of continuous daily 1-km ET estimates and their evaluation against reference data.

2.4.1. Formulation of an interpolation methodology

Continuous estimation of ET was obtained by filling the gaps between remote sensing estimations. We implemented first the two most classical methods based on the linear interpolation of the ratio *R* of ET to an interpolation support *B* that is either the incoming solar radiation (Rg) or the reference evapotranspiration (ET_0). *ET* for a missing day *t* is calculated as

$$ET(t) = R(t).B(t) \tag{10}$$

with

$$R(t) = R(t_k) + \left(R(t_{k+1}) - R(t_k)\right) \frac{t - t_k}{t_{k+1} - t_k} \tag{11}$$

t_k and t_{k+1} (with $t_k < t < t_{k+1}$) corresponding to the days of the previous and the next available "observations".

An interpolation method that more closely follow ET variations is proposed in a second step. It uses alternative estimation of ET that are available at the daily time step, either from other ET products (here, the GLEAM product), a parametric modeling of ET (here, the PAMEAS model) or a combination of both. The procedure is inspired by linear filtering methods considering incremental evolution of ET. In this case, ET estimation for day *t* is obtained by incrementing ET obtained at the previous date *t – 1* considering the change in *B* from day *t – 1* to day *t*:

$$ET(t) = ET(t-1) + w_B(t)[B(t) - B(t-1)] \tag{12}$$

where w_B is a scaling factor accounting for the ratio between *ET* and *B*. For day t_k corresponding to the day with the last available "observation" of ET ($ET(t_k)$), w_B is computed as follow:

$$w_B(t_k) = \frac{ET(t_k)}{B(t_k)} \tag{13}$$

On day *t*, $w_B(t)$ is obtained by interpolating linearly $w_B(t)$ as $R(t)$ in Equation 11 (a mathematical safeguard is implemented when $B(t_k)$ tends towards 0).

Another formulation is proposed when considering several interpolation drivers B. For two drivers B_1 and B_2:

$$ET(t) = ET(t-1) + w_{B_1}(t)[B_1(t) - B_1(t-1)] + w_{B_2}(t)[B_2(t) - B_2(t-1)] \tag{14}$$

Gains $w_{B1}(t)$ and $w_{B2}(t)$ are to be defined from the evolution and/or the proximity of *ET* to B_1 and B_2. They are defined as weighting coefficients between the two sources of interpolation

information B_1 and B_2 considering that ET should be better interpolated by the closest interpolation driver. On day t_k, they are written as:

$$w_{B_1}(t_k) = 1 - \frac{\varepsilon_{B_1}(t_k)}{\varepsilon_{B_1}(t_k) + \varepsilon_{B_2}(t_k)} \quad (15)$$

$$w_{B_2}(t_k) = 1 - \frac{\varepsilon_{B_2}(t_k)}{\varepsilon_{B_1}(t_k) + \varepsilon_{B_2}(t_k)} \quad (16)$$

with

$$\varepsilon_{B_1}(t_k) = |ET(t_k) - B_1(t_k)| \quad (17)$$

$$\varepsilon_{B_2}(t_k) = |ET(t_k) - B_2(t_k)| \quad (18)$$

On day t, $w_{B1}(t)$ and $w_{B2}(t)$ are obtained by linear interpolation between days t_k and t_{k+1} as $R(t)$ in Equation (11). Both $w_{B1}(t)$ and $w_{B2}(t)$ account for the proximity of *B1 and B2* to *ET*. In cases B_i is inter-calibrated with *ET*, $\varepsilon_{Bi}(t_k)$ should be small.

2.4.2. Implementation scheme

In our study, we tested the approach to interpolate ET maps based on the fusion Equation (14). This paragraph outlines the algorithm used and the justification of each step. The different data set and models are presented in detail in the subsequent sections.

2.4.2.1. Calculation of ET

Step 1: calculation of ET maps with E3S (see Section 2.2.1) for each date t_k at which land surface temperature and spectral reflectance are available from MODIS original products.

Step 2: application of the fusion algorithm to generate ET maps on days without E3S estimates. Two interpolation supports are used:

- The GLEAM operational product, which provides estimation of ET every day at 0.25° resolution. ET is computed using a water balance model fed by remote sensing data and meteorological reanalysis (see Section 2.2.2). The advantages of GLEAM are its spatial resolution, which allows capturing mesoscale information on rain, and its heavy use of remote sensing data, in particular the assimilation of microwave radiometer data that enables close monitoring of surface water status.
- Estimates of daily ET at 1 km resolution using a specially-devised model, the PArametric Model for Evapotranspiration in the Agropastoral Sahel (PAMEAS, see Section 2.2.3). The advantage of PAMEAS lies in its parametric form, driven by the Antecedent Precipitation Index (API), representing soil drying kinetics. Concerning the impact of vegetation on ET, PAMEAS is driven by the evolution of f_{COVER} as estimated by MODIS data.

Step 2.1: PAMEAS is calibrated for each pixel at 1 km resolution (P_{1km}) over the time series of ET maps provided by E3S using MODIS data. Four scaling parameters, one for transpiration, one for evaporation and two for the soil drying curve shape are computed for each pixel (see section 2.2.3).

Step 2.2: GLEAM (G_{25km}) is disaggregated at 1 km resolution (G_{1km}) on the basis of ET spatial distribution simulated by PAMEAS (P_{1km}/P_{25km}, P_{25km} being the aggregation of PAMEAS at 25 km spatial resolution):

$$G_{1km}(t) = \frac{P_{1km}(t)}{P_{25km}(t)} G_{25km}(t) \tag{19}$$

Step 2.3: Equation (14) is applied at 1-km resolution with E3S (ET), disaggregated GLEAM ($B_1 = G_{1km}$) and calibrated PAMEAS ($B_2 = P_{1km}$) leading to the fusion between E3S, GLEAM and PAMEAS "Fusion-EGP" as follow:

$$\begin{aligned} ET(t) = E3S(t-1) + \; & w_G(t)[G_{1km}(t) - G_{1km}(t-1)] \\ & + w_P(t)[P_{1km}(t) - P_{1km}(t-1)] \end{aligned} \tag{20}$$

2.4.2.2. Evaluation of the fusion method

Three sets of data are used for the evaluation of the fusion approach:

- ground measurements of ET at one millet field and one fallow site (see section 2.3.1) and simulations of the Simple Soil-Plant-Atmosphere Transfers (SiSPAT) model thoroughly calibrated and validated against field observations which both permitted an evaluation at local scale (see section 2.3.2);
- spatially distributed simulations by an ensemble of 20 LSMs that were performed in the framework of the AMMA Land surface Model Intercomparaison Project Phase 2 (ALMIP2) program (see section 2.3.3). This data set is used for an evaluation at mesoscale by comparing the spatial average of interpolated daily ET over the area to the spatial average of ALMIP2 estimations.

ET derived from the fusion of E3S, GLEAM and PAMEAS, and denoted as "Fusion-EGP", is compared to other interpolation sets:

- "Fusion-EG", from the fusion of E3S with GLEAM only (Equation 12). In this case, GLEAM is not disaggregated and simply super-sampled at MODIS ~ 1 km resolution:

$$E3S(t) = E3S(t-1) + R(t)[G(t) - G(t-1)] \; with \; R(t) = \frac{E3S(t)}{G_{25km}(t)} \tag{21}$$

- "Fusion-EP", from the fusion of E3S with PAMEAS only (Equation 12) :

$$E3S(t) = E3S(t-1) + R(t)[P(t) - P(t-1)] \; with \; R(t) = \frac{E3S(t)}{P(t)} \tag{22}$$

- "Interpol-Rg", from interpolation of E3S with Rg (Equations 10 and 11):

$$E3S(t) = R(t).Rg(t)\ with\ R(t) = \frac{E3S(t_k)}{Rg(t_k)} + \left[\frac{E3S(t_{k+1})}{Rg(t_{k+1})} - \frac{E3S(t_k)}{Rg(t_k)}\right]\frac{t - t_k}{t_{k+1} - t_k} \quad (23)$$

- "Interpol-ET_0", from interpolation of E3S with ET_0 (Equations 1 and 2):

$$E3S(t) = R(t).ET_0(t)\ with\ R(t) = \frac{E3S(t_k)}{ET_0(t_k)} + \left[\frac{E3S(t_{k+1})}{ET_0(t_{k+1})} - \frac{E3S(t_k)}{ET_0(t_k)}\right]\frac{t - t_k}{t_{k+1} - t_k} \quad (24)$$

2.5. Statistical metrics

The performance of each interpolation method was assessed using the bias, the Root Mean Square Error (RMSE), the Nash-Sutcliffe Efficiency (NSE) and the coefficient of determination (R^2).

The impact of the interpolation method alone on ET estimates accuracy is evaluated through a differential RMSE ($RMSE_{int}$) computed as follows:

$$\mathrm{RMSE_{int}} = \sqrt{\mathrm{RMSE^2_{int\_data}} - \mathrm{RMSE^2_{E3S}}} \quad (25)$$

where $RMSE_{int\_data}$ is the RMSE of continuous ET estimates computed for interpolated days and $RSME_{E3S}$ is the intrinsic RMSE of the E3S product which is computed during non-interpolated days.

3. Results

All the fusion and interpolation approaches were applied on the study area over the 2005-2008 period. The results were analyzed both at local scale against field measurements and SiSPAT simulations (section 3.1) and at mesoscale in terms of spatial average against ALMIP2 LSMs simulations (section 3.2).

3.1. Evaluation at local scale

3.1.1. Comparison of interpolation and fusion approaches

In this subsection, comparison of the continuous daily ET estimates obtained after each interpolation or fusion approach against in situ measurements and SiSPAT simulations is analyzed. Overall skill scores of this analysis are summarized in Table 2 and illustrated in Figure 5.

Table 2. Skill scores – bias (in $mm.day^{-1}$), RMSE (in $mm.day^{-1}$), NSE and R^2 – of daily RS-based ET estimates against field observations and SiSPAT simulations over 2005-2008. N is the number of days considered in the comparison.

	Versus observations (N = 1149)				**Versus SiSPAT (N = 1352)**			
	Bias	**RMSE**	**NSE**	**R^2**	**Bias**	**RMSE**	**NSE**	**R^2**
Fusion-EGP	-0.07	0.64	0.78	0.79	-0.05	0.68	0.79	0.80
Fusion-EGP_{LC}	-0.03	0.60	0.81	0.81	-0.01	0.59	0.84	0.85
Fusion-EP	-0.11	0.66	0.77	0.78	-0.10	0.71	0.78	0.79

Fusion-EP_{LC}	-0.05	0.69	0.75	0.76	-0.04	0.65	0.81	0.81
Fusion-EG	-0.02	0.73	0.72	0.73	0.00	0.75	0.75	0.75
Interpol-Rg	-0.07	0.69	0.75	0.76	-0.04	0.75	0.75	0.76
Interpol-ET_0	-0.06	0.74	0.71	0.72	-0.05	0.76	0.74	0.75

The main results provided by Table 2 can be summarized as follows:

- The performances of each method were acceptable, RMSE ranging between 0.59 and 0.76 $mm.day^{-1}$.
- The new interpolation method based on the fusion of E3S, GLEAM and PAMEAS (EGP) provided the best agreement with ground data and SiSPAT simulations as shown by RMSE (0.59 – 0.68 $mm.day^{-1}$), NSE (0.78 – 0.84) and R^2 (0.78 – 0.85) values in Table 2 (actually, the three statistical metrics always provided a similar ranking of the methods, so that only RMSE will be used in the rest of this section).
- The standard interpolation methods based on the interpolation of the ratio of ET to Rg or ET_0 had the lowest performance, in particular in the case of ET_0 (RMSE = 0.74 – 0.76 $mm.day^{-1}$). Remember that these interpolation supports are mainly driven by radiation information and no direct information on precipitation events and drying dynamic were used.
- The fusion methods using PAMEAS as only interpolation support (EP) had intermediary performances (RMSE = 0.65 – 0.71 $mm.day^{-1}$), while the use of GLEAM alone (EG) was providing performance similar as ET_0 (RMSE = 0.73 – 0.75 mm day^{-1}); remember that in this case GLEAM data were used at their native 25 km resolution.
- The local calibration of API parameters on SiSPAT simulations improved the interpolations based on the fusion using PAMEAS (Fusion-EGP_{LC} and Fusion-EP_{LC}) in comparison to the direct calibration of API parameters on E3S estimates (Fusion-EGP and Fusion-EP; see Figure 5).
- All the methods, except Fusion-EG in comparison to SiSPAT simulations, underestimated ET with biases between -0.01 $mm.day^{-1}$ and -0.11 $mm.day^{-1}$, which resulted in underestimations between 4 and 45 $mm.year^{-1}$. No clear differences existed between the methods excepted that the local calibration of API provided lower bias than the calibration of API against E3S data and that biases for Fusion-EP were at least twice larger than for any other method (-0.11 $mm.day^{-1}$).

The most obvious benefits of the fusion approach between E3S, GLEAM and/or PAMEAS compared to classical interpolation methods were observed during the first months of the rainy season (May-June) while images frequency was low and soil drying up was fast. Figure 5 shows that the fusion approach is more able to reproduce surface response to the first rainfall events and consecutive drying up between two E3S estimates even if the amplitude of ET variations were not always correct. One can also observed that local calibration of PAMEAS API parameters allows better depicting the impacts of rainfall events and of soil drying up in the core of the monsoon season (August-September).

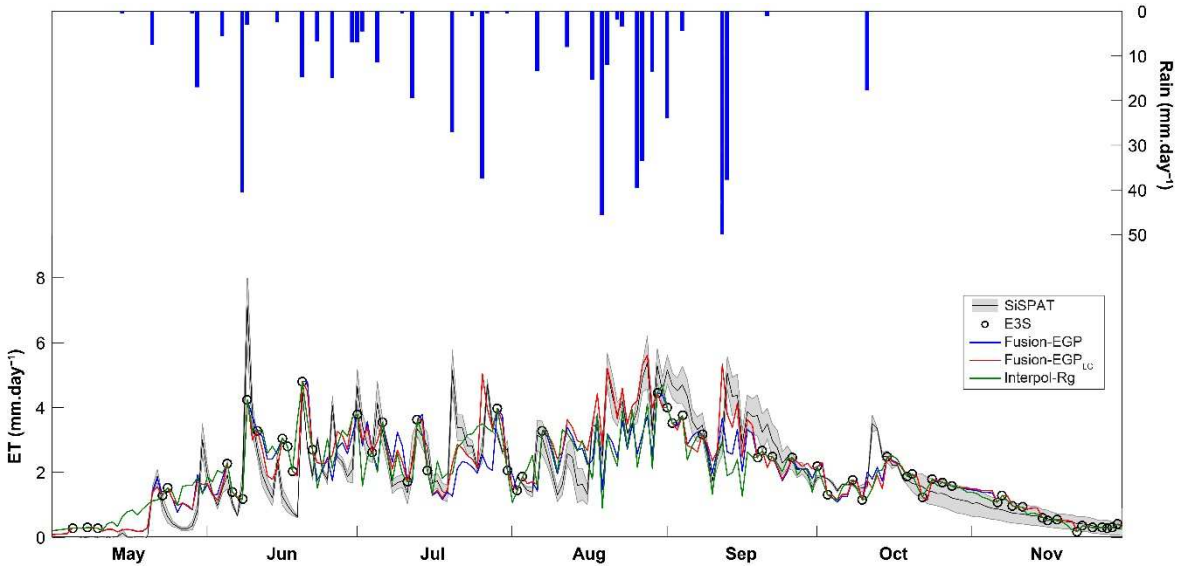

Figure 5. Daily rainfall from raingauge station (bars) and daily ET estimates for 2008 from Fusion-EGP (blue line), Fusion-EGP$_{LC}$ (red line) and Interpol-Rg (green line) versus SiSPAT simulations at local scale (black line and shaded area). The shaded area represents the range between both millet crop and fallow savannah whereas the black line is the average between both plots. The black circles represent non-interpolated dates (E3S).

Most of the differences between interpolation methods on the retrieval of ET was concentrated within the monsoon season. During the dry season, ET was low and not subject to strong variations. Whatever the interpolation method, RMSE were in the order of 0.30 mm.day^{-1} when considering the comparison to SiSPAT simulations and in the order of 0.35 mm.day^{-1} when considering ground observations. Biases were slightly positive, in general lower than 0.05 mm.day^{-1} (not shown). During the monsoon season, the number of available images was low (about 6 images per month in average) compared to the dry season, implying a large number of interpolated data. Periods of up to 20 days had sometimes to be reconstructed. During this season, RMSE ranged between 0.84 and 1.21 mm.day^{-1} which was significantly higher than over the entire study period (note that the ranking of the methods was similar as for the entire period in Table 2). Negative biases were always larger than -0.1 mm.day^{-1} and up to -0.5 mm day^{-1} depending on the interpolation method. Part of these biases came from an underestimation of ET by E3S itself (see Table 4 and Allies et al. (2020) for more details).

3.1.2. Evaluation of interpolated ET versus E3S estimates

In order to evaluate the performance of the interpolation methods, Tables 3 and 4 and Figure 6 present separated evaluations of ET retrievals obtained (i) for days with available remote sensing data with E3S (Table 4 and blue points in Figure 6) and (ii) for interpolated ET between available E3S estimates (Table 3 and red points in Figure 6). The impact of the interpolation procedure on the performance of the interpolation was evaluated through RMSE$_{int}$ (see Equation 24), the differential RMSE between the errors related to E3S (RMSE$_{E3S}$) and the errors calculated on interpolated data (RMSE$_{int_data}$). RMSE$_{E3S}$ (0.47 – 0.46 mm.day^{-1}) were strongly lower than the overall values of RMSE presented in Table 2.

572 The impact of the interpolation procedure was either of similar magnitude ($RMSE_{int}$ between
573 0.43 and 0.58 for Fusion-EGP and Fusion-EGP_{LC}) or larger (up to 0.69 $mm.day^{-1}$ for Interpol-
574 ET_0). The observation of the differences between the bias for E3S and the bias for the
575 interpolated data indicated that the interpolation methods generally induce some
576 underestimations in particular when the evaluation is performed against SiSPAT simulations.
577 This underestimation was larger for Fusion-EP (- 0.13 $mm.day^{-1}$) and in general more limited
578 for Fusion-EGP and Fusion-EG. The local calibration of API (Fusion EGP_{LC} and Fusion
579 EP_{LC}) was also reducing both bias and $RMSE_{int}$ generated by the interpolation procedures.

580 **Table 3.** Skill scores – bias (in $mm.day^{-1}$), $RMSE_{int\_data}$ (in $mm.day^{-1}$), $RMSE_{int}$ (in $mm.day^{-1}$)
581 – of daily RS-based interpolated ET estimates against field observations and SiSPAT
582 simulations over 2005-2008. N is the number of days considered in the comparison.

	Versus observations (N = 851)			**Versus SiSPAT (N = 1016)**		
	Bias	**$RMSE_{int\_data}$**	**$RMSE_{int}$**	**Bias**	**$RMSE_{int\_data}$**	**$RMSE_{int}$**
Fusion-EGP	-0.08	0.69	0.51	-0.06	0.74	0.58
Fusion-EGP_{LC}	-0.03	0.64	0.43	-0.03	0.63	0.43
Fusion-EP	-0.13	0.71	0.53	-0.13	0.77	0.62
Fusion-EP_{LC}	-0.05	0.75	0.58	-0.06	0.71	0.54
Fusion-EG	-0.01	0.80	0.65	-0.00	0.82	0.68
Interpol-Rg	-0.07	0.75	0.58	-0.06	0.82	0.68
Interpol-ET_0	-0.06	0.80	0.65	-0.07	0.83	0.69

583 **Table 4.** Skill scores – bias (in $mm.day^{-1}$), $RMSE_{E3S}$ (in $mm.day^{-1}$) – of daily RS-
584 based non-interpolated ET estimates (E3S only) against field observations and
585 SiSPAT simulations over 2005-2008.). N is the number of days considered in the
586 comparison.

	Versus observations (N = 298)		**Versus SiSPAT (N = 336)**	
	Bias	**$RMSE_{E3S}$**	**Bias**	**$RMSE_{E3S}$**
E3S (non-interpolated)	-0.05	0.47	-0.02	0.46

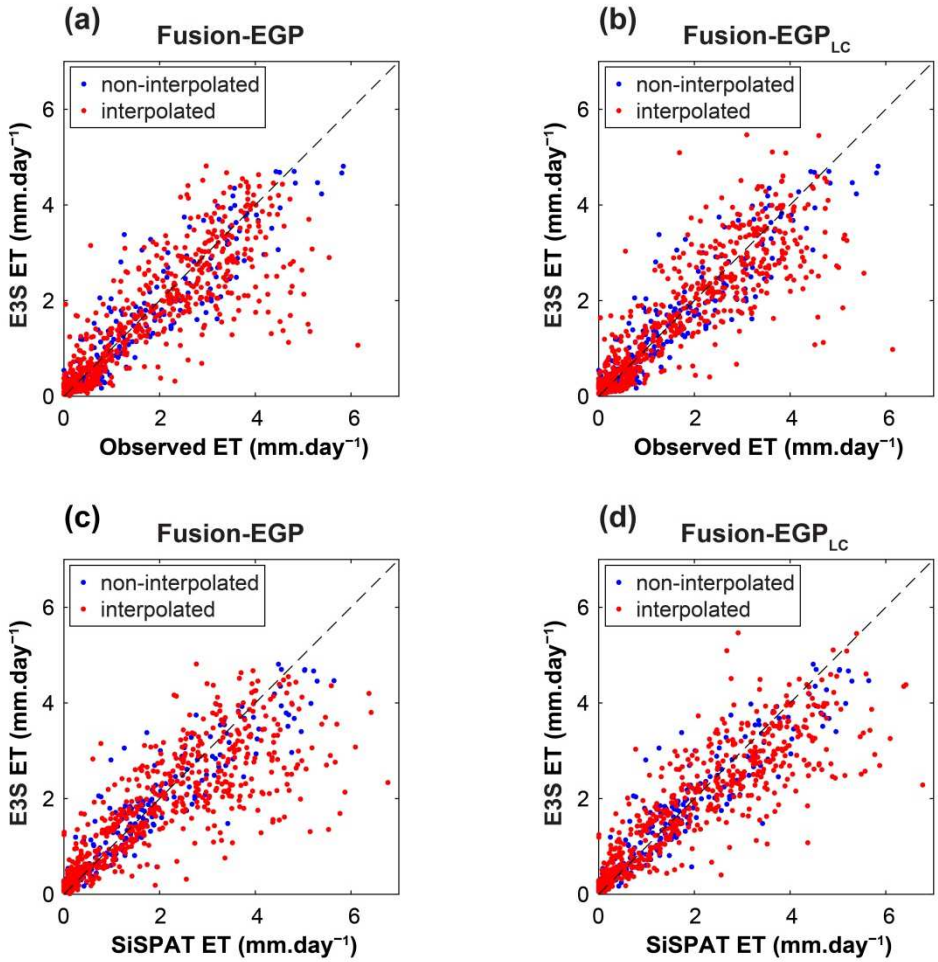

Figure 6. Daily ET estimates from the fusion between E3S, GLEAM and PAMEAS without (Fusion-EGP; a, c) and with (Fusion-EGP$_{LC}$; b, d) local calibration of PAMEAS API parameters versus eddy covariance measurements (top row panel) and SiSPAT simulations (bottom row panel) over 2005-2008. The blue points represent E3S estimates for days with available remote sensing data and the red points are interpolated ET values between available E3S estimates.

3.1.3. Residual error analysis of ET estimates

Residual errors (ε_{ET} = predicted ET – SiSPAT ET) for each fusion or interpolation method are computed at the Wankama pixel scale. The distributions of ε_{ET} against standard deviation of SiSPAT simulated ET between two consecutive E3S estimates are shown in Figure 7. The boxplots show, for each approach, the interquartile range of ε_{ET} for the ranges of SiSPAT standard deviation. One can observe that ε_{ET} interquartile range globally increases when the SiSPAT standard deviation increases. For low standard deviation ($\leq$ 0.05 mm.day^{-1}) between two consecutive E3S estimates, ε_{ET} is still low (-0.4 mm.day^{-1} < ε_{ET} < 0.9 mm.day^{-1}) for every fusion or interpolation method and no significant differences in ε_{ET} distribution is observed between them. All of them also show a ε_{ET} slightly positively skewed for SiSPAT standard deviation less than 0.05 mm.day^{-1}. For the range]0.05;0.5] mm.day^{-1} of SiSPAT standard deviation, the ε_{ET} distribution is quite symmetric for each interpolation and fusion method

even if Interpol-Rg and Interpol-ET_0 both show an underestimation trend for values outside the whiskers range (Figures 7. f and g). Main differences in the distribution of ε_{ET} between fusion and interpolation methods are observed for SiSPAT standard deviation greater than 0.5 $mm.day^{-1}$. For such values, both Interpol-Rg and Interpol-ET_0 generally display a larger interquartile range than all of the fusion approaches. For these interpolation methods, the distribution of ε_{ET} is negatively skewed for standard deviation ranges]0.5;1] and]1;1.5] $mm.day^{-1}$ and rather positively skewed for standard deviation greater than 1.5 $mm.day^{-1}$ (Figures 7. F and g). Fusion-EG shows a symmetric ε_{ET} distribution for standard deviation range]0.5;1] $mm.day^{-1}$, negatively skewed for range]1;1.5] $mm.day^{-1}$ and slightly positively skewed for standard deviation > 1.5 $mm.day^{-1}$ (Figure 7. e). Fusion-EP is characterized by a negatively skewed ε_{ET} distribution for ranges]0.5;1] and]1;1.5] $mm.day^{-1}$ and symmetric for standard deviation > 1.5 $mm.day^{-1}$ (Figure 7. c). Fusion-EGP shows a negatively skewed ε_{ET} distribution for ranges]0.5;1] and]1;1.5] $mm.day^{-1}$ and a positively skewed distribution for standard deviation > 1.5 $mm.day^{-1}$ (Figure 7. a). One can observe that the local calibration of PAMEAS API parameters reduces the ε_{ET} interquartile range and generally also reduces the skewness of the ε_{ET} distribution (Figures 7. b and d). Indeed, Fusion-EGP_{LC} and Fusion-EP_{LC} clearly show a lower dispersion of ε_{ET}, as well as an average of ε_{ET} close to 0. This confirms better performances of locally calibrated fusion approaches as shown in sections 3.1.1 and 3.1.2.

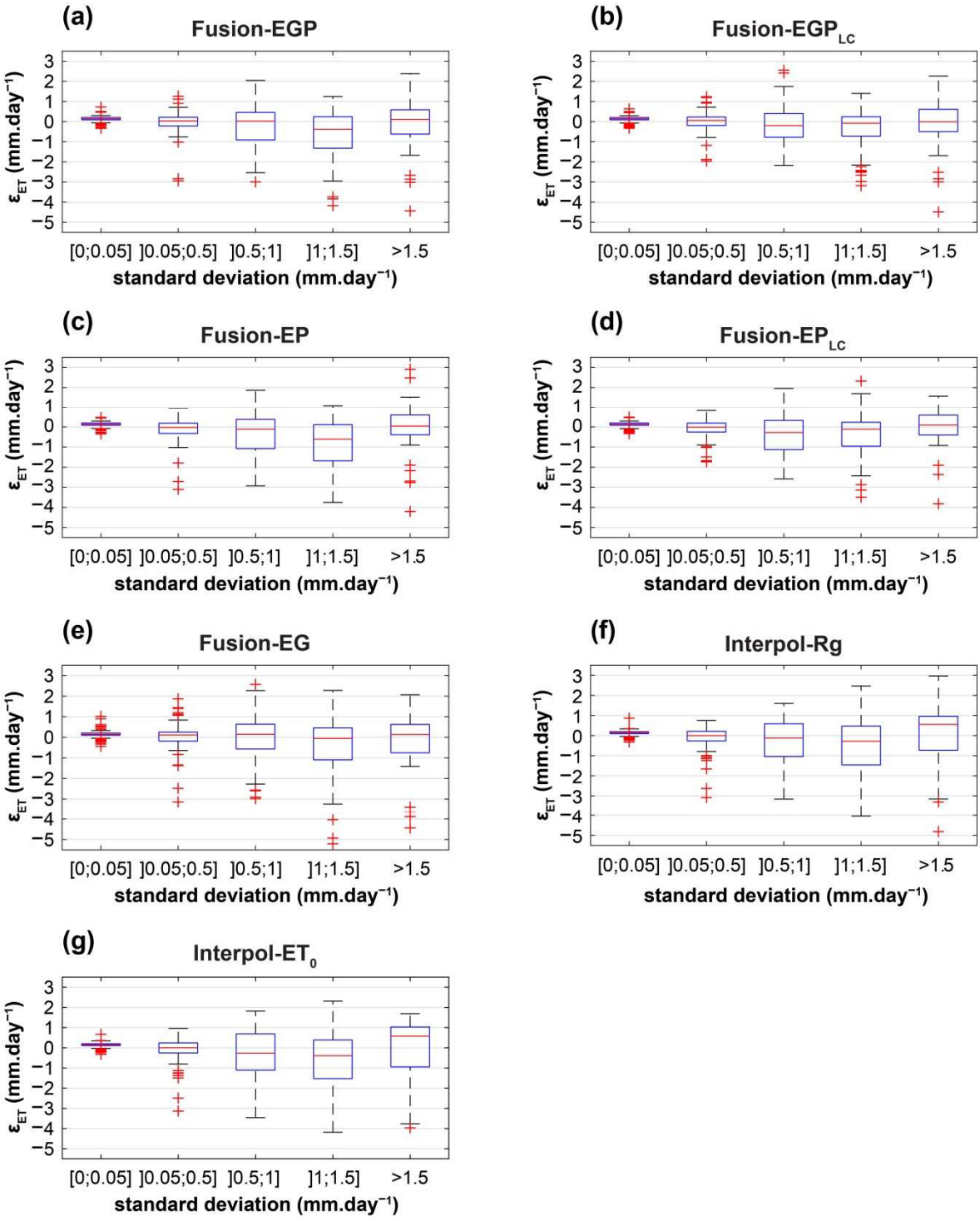

Figure 7. Boxplots showing the distribution of residual errors in derived ET (ε_{ET}) from Fusion-EGP (a), Fusion-EGP$_{LC}$ (b), Fusion-EP (c), Fusion-EP$_{LC}$ (d), Fusion-EG (e), Interpol-Rg (f) and Interpol-ET$_0$ (g) in relation to the SiSPAT ET standard deviation between two consecutive E3S estimates. Only interpolated values are considered. The red line in each box is the median of ε_{ET} values, the lower bar of the box is the first quartile and the upper one is the third quartile. The lower whisker bar corresponds to the maximum between minimum ε_{ET} and the first quartile minus 1.5-fold the interquartile range. The upper whisker bar

corresponds to the minimum between maximum ε_{ET} and the third quartile plus 1.5-fold the interquartile range and red plus signs are values outside these whiskers.

3.2. Evaluation at mesoscale

In this subsection, comparison of the continuous daily ET estimates obtained after each interpolation or fusion approach against ensemble average of ALMIP2 LSMs simulations is analyzed. The comparison was done by considering spatial averages over the whole ALMIP2 domain (20 800 km²). Overall skill scores of this analysis are summarized in Table 5 and illustrated in Figures 8 and 9.

Table 5. Skill scores – bias (in mm.day^{-1}), RMSE (in mm.day^{-1}), NSE and R^2 – of daily RS-based ET estimates against the ensemble average of ALMIP2 LSMs simulations over 2005-2008. The comparison was performed over 1458 days.

	Bias	RMSE	NSE	R^2
Fusion-EGP [1]	0.03	0.46	0.87	0.88
Fusion-EGP$_{LC}$ [2]	0.06	0.45	0.88	0.89
Fusion-EP [3]	-0.01	0.52	0.84	0.84
Fusion-EP$_{LC}$ [4]	0.06	0.56	0.82	0.83
Fusion-EG [5]	0.10	0.47	0.87	0.87
Interpol-Rg [6]	-0.02	0.59	0.79	0.80
Interpol-ET$_0$ [7]	-0.03	0.64	0.77	0.78

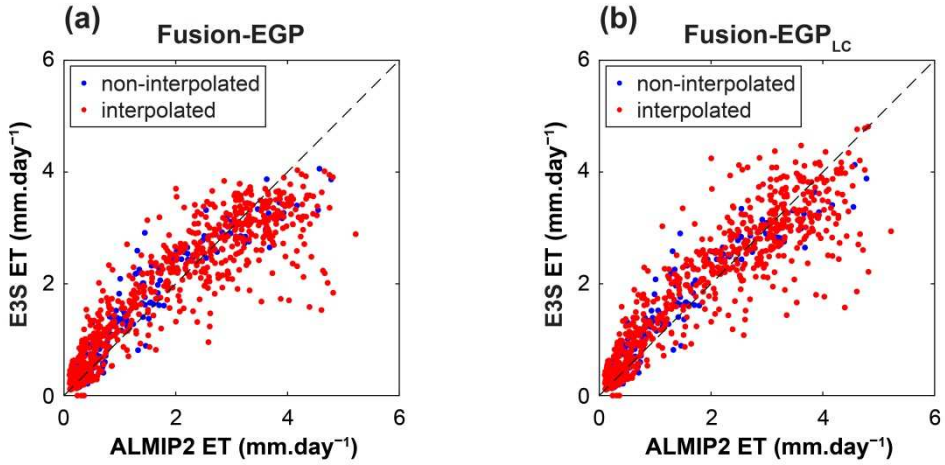

Figure 8. Daily ET estimates from the fusion between E3S, GLEAM and PAMEAS without (Fusion-EGP; a) and with (Fusion-EGP$_{LC}$; b) local calibration of PAMEAS API parameters versus the ensemble average of ALMIP2 LSMs over 2005-2008. The non-interpolated dates (blue points) are defined as those for which more than 75 % of pixels of the E3S image are available over the study site.

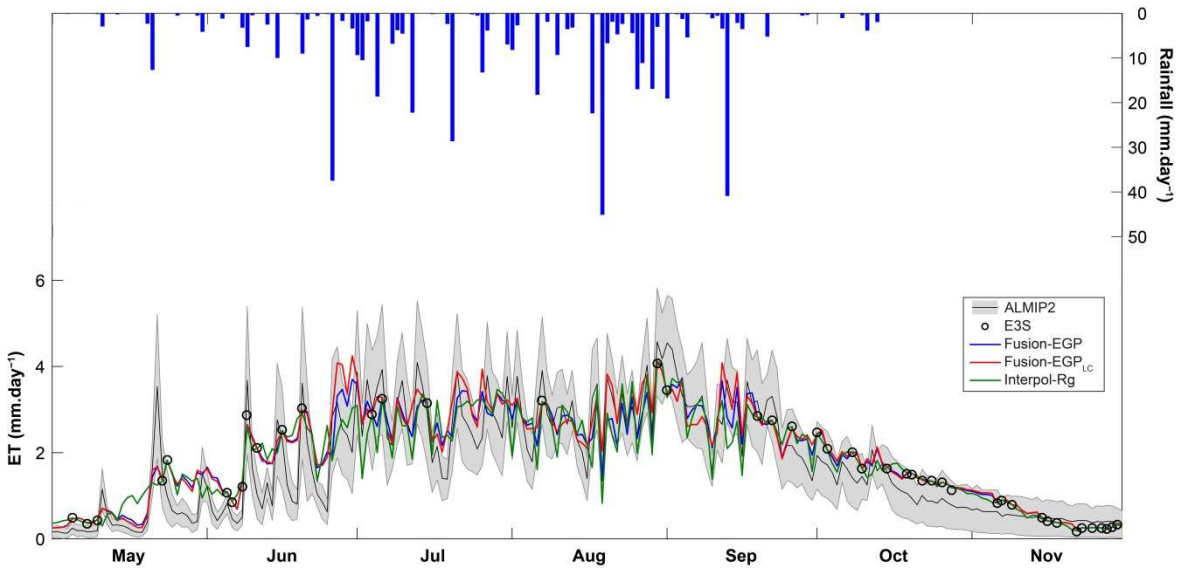

Figure 9. Mesoscale average of daily rainfall from raingauge stations (bars) and ET estimates for 2008 from Fusion-EGP (blue line), Fusion-EGP$_{LC}$ (red line) and Interpol-Rg (green line) versus ALMIP2 simulations at mesoscale. The shaded area represents the standard deviation of the 20 ALMIP2 LSMs whereas the black line is the average of the 20 ALMIP2 LSMs. The non-interpolated dates (E3S) are defined as those for which more than 75 % of pixels of the E3S image are available over the study site.

Many results of the mesoscale comparison were in line with those obtained at local scale on the Wankama pixel (Table 5):

- The best performances were obtained with the fusion method using both GLEAM and PAMEAS information (EGP).
- The standard interpolation procedures (Rg and ET_0) had the lowest performances.
- The fusion method based on PAMEAS only had intermediary performance whereas the one based on GLEAM only showed quite similar results as those obtained with dual-source fusion approaches.
- Main benefits of the fusion approach (Fusion-EGP and Fusion-EGP$_{LC}$) was observed during the first months of the rainy season (Figure 9) in the depiction of drying up phases between two consecutive rainfall events (drying up amplitude and timing), showing the interest of interpolation supports including information on either rainfall or surface soil moisture fields.
- The main discrepancies between retrieved ET and ALMIP2 LSMs occurred during the monsoon season and were characterized by a significant underestimation.

There were however significant differences:

- RMSE were significantly lower (e.g. 0.46 for Fusion-EGP to be compared to 0.64-0.68 at local scale).
- The local calibration of PAMEAS API parameters (Fusion-EGP$_{LC}$ and Fusion-EP$_{LC}$) had low impact on the performance (see Figure 8 and Table 5; remember that in this

case the API parameters obtained by calibration against SiSPAT simulations over the millet field and the fallow were used all over the studied domain) but tended to positively increase the bias.

- No clear trend existed for the bias value versus the interpolation method.
- The direct impact of the interpolation procedure ($RMSE_{int}$; Table 6) was always larger than the errors generated by the application of E3S (Table 7). The difference was only slight when considering E3S, GLEAM and PAMEAS together ($RMSE_{E3S}$ = 0.31 $mm.day^{-1}$, $RMSE_{int}$ = 0.35 – 0.38 $mm.day^{-1}$) but it increased when considering other methods and in particular standard interpolation with Rg ($RMSE_{int}$ = 0.56 $mm.day^{-1}$) and even worse for ET_0 (0.63 $mm.day^{-1}$). For the latter, the interpolation procedure was responsible of two thirds of the difference between RS-based ET estimates and ALMIP2 LSMs simulations.

Table 6. Skill scores – bias (in $mm.day^{-1}$), $RMSE_{int\_data}$ (in $mm.day^{-1}$), $RMSE_{int}$ (in $mm.day^{-1}$) – of daily RS-based interpolated ET estimates against the ensemble average of ALMIP2 LSMs simulations over 2005-2008. The interpolated days (N) are defined as those for which less than 75 % of pixels of the E3S image are available over the study site.

	Versus ALMIP2 LSMs (N = 1177)		
	Bias	**$RMSE_{int\_data}$**	**$RMSE_{int}$**
Fusion-EGP	0.02	0.49	0.38
Fusion-EGP_{LC}	0.06	0.47	0.35
Fusion-EP	-0.03	0.56	0.47
Fusion-EP_{LC}	0.06	0.60	0.51
Fusion-EG	0.11	0.50	0.39
Interpol-Rg	-0.04	0.64	0.56
Interpol-ET_0	-0.06	0.70	0.63

Table 7. Skill scores – bias (in $mm.day^{-1}$), $RMSE_{E3S}$ (in $mm.day^{-1}$) – of daily RS-based non-interpolated ET estimates (E3S only) against ensemble average of ALMIP2 LSMs simulations over 2005-2008. Non-interpolated days (N) are defined as those for which more than 75 % of pixels of the E3S image are available over the study site.

	Versus ALMIP2 LSMs (N = 281)	
	Bias	**$RMSE_{E3S}$**
E3S (non-interpolated)	0.06	0.31

4. Discussion

In this study, we introduced a new method to interpolate daily evapotranspiration between available remote sensing estimates. The objective was to provide continuous estimates of ET as required for many hydrological applications. The method was applied to MODIS estimates of ET at the kilometer resolution over the Niamey area in Niger. Broadly speaking, our study shows that over the whole season, cumulative ET is fairly well represented with simple Rg-

based or ET_0-based interpolation, but that intra-seasonal dynamics require something a little more complex. In that sense, the new methodology, based on a data fusion algorithm, provided better results than the standard methods that have been classically used for interpolating ET estimates based on the interpolation of the ratio of ET to Rg or ET_0. The improvement was generally around 0.1 in terms of NSE, which indicates a better description of the variations of daily ET. This was clearly illustrated by the better depiction of the first precipitation events at the beginning of the rainy period (Figure 5). During the monsoon season, while the number of E3S estimates was limited in reason of the low availability of MODIS data, the improvement was also substantial. The fusion method used information on soil drying up and rain events which were not available with the standard interpolation method.

It is difficult to compare our results to those obtained in previous studies as almost no analysis was published comparing standard methodologies based on the interpolation of simple ratio as defined by Equations 10 and 11 to methodologies introducing information on the timing of precipitations and drying kinetics. When considering analysis of the interpolation of ET on in-situ datasets, RMSE ranging between 0.2 and 0.9 $mm.d^{-1}$ were obtained for a large range of ecosystems and climates over Contiguous United States and the Mediterranean (Delogu et al., 2021; Guillevic et al., 2019). The lowest values were obtained under semi-arid conditions, over wheat crops in Morocco (Delogu et al., 2021) and woody savannahs in Southwestern USA (Guillevic et al., 2019) which were characterized by low daily ET values. Larger RMSE values, above 0.4 $mm.d^{-1}$, were obtained in wetter conditions, in particular for industrial crops, grasslands and forests. In our study, the values of $RMSE_{int}$, which quantify the impact of the interpolation method alone (Table 3), were falling in the middle of that range of performances (0.65 $mm.d^{-1}$ when using ET_0 and 0.58 $mm.d^{-1}$ when using Rg). $RMSE_{int}$ for the fusion method was significantly lower (0.51 $mm.d^{-1}$). When considering evaluation of continuous estimates of daily ET from satellite data (combining errors on interpolation together with errors due to the estimation of ET on days with remote sensing data) the RMSE values given in Table 2 were lower than found in previous studies: 0.8 $mm.d^{-1}$ over a dry saltmarsh scrubland (interpolated ET/Rg ratio ; Gallego-Elvira et al., 2013), 1.1 to 1.8 $mm.d^{-1}$ over agricultural areas (MODIS/Landsat fusion ; Cammalleri et al., 2013), 0.9 $mm.d^{-1}$ over vineyards (GOES/MODIS/Landsat fusion ; Semmens et al., 2016). Conversely to our analysis, none of these studies was using information on precipitation and drying kinetics.

In any situation, the fusion method based on two interpolation supports (Fusion-EGP), namely GLEAM and PAMEAS, provided better results than the use of one interpolation support. At local scale, the performance of Fusion-EG was similar to the performance of the standard interpolation methods (Table 2). At mesoscale (vs. ALMIP2 ensemble simulations), they were close to those of Fusion-EGP (Table 5). On its side, Fusion-EP, based on PAMEAS simulations, had always lower performance than Fusion-EGP. At local scale (vs. flux tower measurements), this seemed to demonstrate that both supports were providing interesting information for interpolating ET estimates while at mesoscale, GLEAM seemed to provide most of the information. This may be related to the impact of the calibration of PAMEAS over the whole domain. Indeed, we shown at local scale, that when PAMEAS API parameters

were calibrated on ground information (here SiSPAT simulations) the performance of fusion methods using PAMEAS were increased. In our work, it was not possible to calibrate the API formulation over different locations. The possibility to use an API calibrated on ground data for different locations and, in particular, different land cover and soil types should be investigated in the future. The differences in the performance of both mono-interpolation support methods at local scale gave also an indication of the interest of using interpolation support at the finer resolution (GLEAM in Fusion-EG is used at its original resolution, i.e. 25 km, while it is disaggregated at the kilometer resolution in Fusion EGP).

Our results also illustrated that the interpolation process itself was usually generating larger errors in the derivation of continuous estimates of ET than the direct estimation of ET from remote sensing data. In the best case (fusion of E3S with GLEAM and PAMEAS at local scale) both errors had almost similar level. This indicates that more efforts have to be done for improving interpolation procedures. Our study participated to these efforts, in particular by showing that improvements can be obtained when introducing information on the kinetics of soil drying up and on the occurrence of precipitation events (and probably the amount of rainfall water also). Compared to the number of studies proposing and analyzing ET models, the literature on ET interpolation is reduced to a limited number of articles. Most of them only analyzed the results of the standard interpolation methods (Alfieri et al., 2017; Delogu et al., 2021; Guillevic et al., 2019; Lagouarde et al., 2013, 2010). This has maybe been related to the difficulties for obtaining accurate information on rain occurrence and amount in a distributed way over large areas, while information on incoming solar radiation and on ET_0 have been more easily available. Actually, various precipitation products are available nowadays. They are derived from interpolation of gauge observations (e.g. GPCC (Schneider et al., 2014), CRU (Chen et al., 2008)), satellite data (e.g. CHOMPS (Joseph et al., 2009), CMORPH (Joyce et al., 2004)), combination of satellite and gauge data (e.g. CHIRPS (Funk et al., 2015), TMPA 3B42 (Huffman et al., 2007)), meteorological reanalysis (ERA-Interim (Dee et al., 2011), NCEP-CFSR (Saha et al., 2010)) or from the combination of satellite data, gauge measurements and atmospheric model reanalysis (e.g. MSWEP (Beck et al., 2017)).

The new method developed in this study was applied for interpolating ET estimated from MODIS data over a Sahelian area. One can wonder what would be the applicability of the method over other areas, other climate or other sensors having different revisit characteristics. Concerning climate, the number of available MODIS data for estimating ET during the monsoon season is very limited implying the reconstruction of ET for a very large proportion of days (about 75 % of ET data have been interpolated in this study). In this situation, the new method proved to be efficient in comparison to the standard interpolation methods and we can anticipate it would perform correctly in situations with a larger density of available data. This also indicates that the method could be transferred to the interpolation of ET derived from sensors onboard Landsat platforms with a long revisit time. Nonetheless, in the case of a higher number of images, the performance gain compared to a simpler interpolation method would probably become too low given the higher complexity of the fusion method developed in the present study.

One of the main advantages of the method relies on the integration of precipitation data that provide essential information on the variations of ET during long period. This is in line with the results obtained by Delogu et al. (2021) over a large number of in-situ datasets. However, an analysis of the interest of such method over very long period, up to several weeks, without ET data, as it can happen when using Landsat data, still has to be investigated. One can anticipate that in such situation the performance of the method would greatly depends on the quality of the calibration of an interpolation support such as PAMEAS. It should also be noticed, that precipitation information is not sufficient for following the alternation of wetting / drying events over irrigated areas. Information on irrigation calendar and amounts is very difficult to obtain. In these cases, the interest of using remote sensing data sensitive to surface soil moisture, as microwave backscattering, has to be investigated. GLEAM is already integrating microwave data but with a spatial resolution not suitable for the detection of irrigation events. The use of microwave data such as those provided by Sentinel 1A and 1B with a revisit cycle of 6 days might be used for detecting at least some of the irrigation events and also for helping in the calibration of interpolation support as PAMEAS. Another advantage of the methodology relies on the use of models that describe the evolution of surface water status and provide information on the kinetics of ET over time. In our case such information is provided either by PAMEAS at the pixel scale and GLEAM at mesoscale. Other surface water balance models could be used, such as the SimpKcET model (Olioso et al., 2019; Ollivier et al., 2021) which is developed from the FAO56 method (Allen et al., 1998) and can be applied to a wide range of ecosystems.

5. Conclusion

The purpose of this work was to build a multi-resolution and multi-source remote sensing data fusion approach to produce continuous daily ET maps at 1 km resolution in Sahelian areas. The proposition of such an approach appeared to be a key issue for Sahelian areas given the inefficiency of standard temporal interpolation techniques for long return intervals and WAM-linked cloud cover during the rainy season. The proposed methodology relied on the use of the GLEAM global ET product and a parametric model named PAMEAS as a normalized basis to fill gaps in MODIS-based E3S ET estimates between two clear sky days acquisition. The fusion approach was compared to more classical temporal interpolation techniques involving the linear interpolation of the ratio between ET and Rg or ET_0. RS-based ET estimates were evaluated in southwest Niger during the 2005-2008 period at (i) the pixel scale against eddy-covariance measurements and simulations of a beforehand calibrated/validated land surface model named SiSPAT, (ii) at mesoscale against simulations of the 20 regional ALMIP2 LSMs as a reference basis. At pixel scale, fusion-based ET estimates showed good skill scores compared both to SiSPAT simulations (RMSE = 0.68 $mm.day^{-1}$, NSE = 0.79, R^2 = 0.80) and field measurements (RMSE = 0.64 $mm.day^{-1}$, NSE = 0.78, R^2 = 0.79). Compared to ET_0- and Rg-based interpolation techniques, the fusion approach allowed significantly reducing RSME and enhancing NSE and R^2 with respect to observations and SiSPAT simulations. The main benefits of the fusion algorithm are observed during the first months of the rainy season in its capacity to reproduce the alternation between ET peaks and drying up phases. Residual error analysis showed that the fusion approach reduces the interpolated RS-

based ET error for high values (> 0.5 mm.day^{-1}) of observed ET standard deviation between two available estimates. Quite similar results are obtained at mesoscale compared to the mesoscale mean of ALMIP2 models simulations showing the spatial consistency of the here developed fusion algorithm. We also show that fusion-based ET estimates are in better agreement with LSMs references at both local and mesoscale than those based on either GLEAM or PAMEAS estimates alone, showing the benefit of the multi-source fusion approach. The local calibration of PAMEAS API parameters substantially improves performance of the fusion approach at local scale without modifying its performance at mesoscale. This last point highlights the interest of a multi-point local calibration of the model against surface soil moisture measurements for future improvements of the fusion approach. It is believed that such a fusion approach is particularly appealing to take advantage of multi-source and multi-resolution datasets to produce consistent continuous ET estimates. This fusion technique will be implemented in other mesoscale areas in Sahelo-Saharan Mali and Sudanian Benin, instrumented in the framework of the AMMA-CATCH NOS, to evaluate the replicability of the methodology. Finally, given the need of fine scale ET estimates and the recent development of disaggregation algorithms, we suggest that such a fusion approach could be used as a first stage in a disaggregation chain to ensure better consistency between continuous multi-resolution ET estimates.

Funding: The first author's Ph.D. was financed by a student research grant from GAIA Doctoral School at University of Montpellier (https://gaia.umontpellier.fr/). This work also received support from French Centre National d'Études Spatiales (CNES) through both TOSCA projects EVASPA v3.0 and PITEAS (Production par Interpolation Temporelle de l'Evapotranspiration journalière issue de l'infrarouge thermique à l'Aide de données auxiliaireS) as well as from PNTS programme of the French Centre National de Recherche Scientifique in the framework of the PRETAO project (PRoduits d'EvapoTranspiration en Afrique de l'Ouest).

Acknowledgments: The ground data set was acquired and disseminated by the AMMA-CATCH NOS (www.amma-catch.org) in the framework of the AMMA (African Monsoon Multidisciplinary Analysis) Program. Special thanks are thus due for the AMMA-CATCH team members. Authors thanks Monique Oï, Jean-Philippe Chazarin, Ibrahim Maïnassara, Florent Arpin-Pont, Hélène Barral and all members of the local IRD team in Niger for having provided us long series and good quality ground measurements. We also thank the Land Processes Distributed Active Archive Centre (LP DAAC) for the availability of MODIS data and the Global Land Evaporation Amsterdam Model team for the availability of GLEAM evapotranspiration product. Lastly, authors are grateful to the members of the ALMIP2 project for providing the models simulations and for their very useful analysis of models behaviors and performances.

Appendix A – Gap filling method of Velluet (2014)

In a first step, an average daily cycle of ET is defined for each day of a "typical" year at the measurement timescale (here 30 min). The latter is estimated computing 15-day moving average of observed ET over the entire measurements period Δy (here Δy = 7 years from y_1 =

2005 to y_n = 2011). Thus $15\Delta y$ days of measurements are averaged to estimate a typical profile of a daily ET cycle at a given day d_0 ($ET_{d0}(t)$ *with* $0 \leq t \leq 23.5$ *hours):*

$$ET_{d_0}(t) = \frac{1}{15\Delta y} \sum_{d=d_0-7}^{d_0+7} \sum_{y=2005}^{2011} ET_{y,d}(t) \ with\ \Delta y = 7 \quad \text{(A.1)}$$

One defines $T(y,d)$ as moments for which measurement of $ET_{y,d}(t)$ is available for day d of year y. For each day d of each year y, one defined $f(y,d)$ as the ratio between the daily sum of the typical daily cycle at measurements available moments and the daily sum of the complete typical daily cycle:

$$f(y,d) = \frac{\sum_{T(y,j)} ET_d(t)}{\sum_{t=0}^{23h30} ET_d(t)} \quad \text{(A.2)}$$

If $f(y,d)$ is strictly greater than 2/3, observed daily ET of day d of year y, written $\langle ET_{y,d} \rangle$, is derived from:

$$\langle ET_{y,d} \rangle = \frac{1}{48} \frac{1}{f(y,d)} \sum_{T(y,d)} ET_{y,d}(t) \quad \text{(A.3)}$$

Else if $f(y,d)$ is less or equal to 2/3, daily gapfilling is not performed.

Appendix B - Land surface models used in the ALMIP2 exercise

Model name	Institute and reference
CLASS[1]	Climate Research Division, Environment Canada, Toronto, Canada (Verseghy, 1991)
CLM_CLM4[2]	Department of Atmospheric Sciences at National Taiwan University, Taipei, Taiwan (Lawrence et al., 2011)
CLM_ECOV2[3]	Same as CLM_CLM4
CLM_CN[4]	Same as CLM_CLM4
CLSM[5]	METIS Paris, France (Koster et al., 2000)
CLSM-NASA	GMAO, NASA/GSFC, Greenbelt, MD, USA (Koster et al., 2000)
HTESSEL[6]	ECMWF, Reading, UK (Balsamo et al., 2011)
CTESSEL[7]	ECMWF, Reading, UK (Boussetta et al., 2013)
ISBA[8]	CRNM-GAME, Toulouse, France (Noilhan and Mahfouf, 1996)
JULES[9]	CEH, Wallinford, UK (Best et al., 2011; Clark et al., 2011)
LISMosaic[11]	GMAO, NASA/GSFC, Greenbelt, MD, USA (Koster and Suarez, 1992)
LISNoah33[12]	GMAO, NASA/GSFC, Greenbelt, MD, USA (Decharme et al., 2009)
MATSIRO[13]	Institute of Industrial Science, The University of Tokyo, Japan (Takata et al., 2003)
ORCHIDEE_dyn[14]	LSCE, Gif-sur-Yvette, France (d'Orgeval et al., 2008)
ORCHIDEE_f[15]	LMD, Paris, France (d'Orgeval et al., 2008)
SETHYS[16]	LSCE, Gif-sur-Yvette, France (Saux-Picart et al., 2009)
SIBUC[17]	Rikagaku Kenkyusho Advanced Institute for Computational Science, Kobe, Japan
SPONSOR[18]	Institute of Geography, Russian Academy of Sciences, Moscow, Russia (Shmakin, 1998)
STEP[19]	GET, Toulouse, France (Pierre et al., 2016)
SWAP[20]	Institute of Water Problems, Moscow, Russia (Nasonova et al., 2015)

[1]CLASS stands for the Canadian Land Surface Scheme.

[2]CLM stands for the Community Land Model.

[3]_ECOV2 stands for ECOCLIMAP2, version 2.

[4]_CN represents carbon (C) and nitrogen (N).

[5]CLSM stands for the Catchment LSM.

[7]HTESSEL stands for the Hydrology Tiled ECMWF Scheme of Surface Exchanges over Land.

[8]CTESSEL stands for the Carbon Tiled ECMWF Scheme of Surface Exchanges over Land.

[9] ISBA stands for Interactions between Soil, Biosphere, and Atmosphere.

[10]JULES stands for the Joint UK Land Environment Simulator.

[11]LISMosaic stands for Mosaic with Land Information System.

[12]LISNoah33 stands for Noah with Land Information System.

[13]MATSIRO stands for the Minimal Advanced Treatments of Surface Interaction and Runoff model.

[14]ORCHIDEE_dyn stands for Organizing Carbon and Hydrology in Dynamic Ecosystems (ORCHIDEE) with dynamic vegetation.

[15]ORCHIDEE_f stands for ORCHIDEE with forced vegetation.

[16]SETHYS stands for Suivi de l'Etat Hydrique des Sols.

[17]SIBUC stands for the Simple Biosphere Model including Urban Canopy.

[18]SPONSOR stands for the Semi-distributed Parameterization Scheme of the Orography-induced hydrology model.

[19]STEP stands for the Sahelian Transpiration Evaporation Productivity model.

[20]SWAP stands for the Soil, Water, Atmosphere, and Plant.

Appendix C – Local calibration of PAMEAS against SiSPAT reference simulations

PAMEAS was calibrated against the simulations of SiSPAT on the 2005-2012 period. Calibrated values of parameters used in the formulations of API, E and T are presented in Table C.1 for the millet field and the fallow respectively. Calibration was performed to minimize Root Mean Square Error (RMSE) and maximize Nash-Sutcliffe Efficiency (NSE) and coefficient of determination (R^2) together to find the set of parameters providing the best trade-off.

Table C.1. PAMEAS' parameters values used in this study for the millet crop and the fallow plots

	Millet	**Fallow**
API (ω_1; ω_2)	3.8; 4	4; 3.5
E (ρ_1)	0.69	0.84
T (ρ_2)	1.05	0.74

Very good performances are observed between simulated API from PAMEAS and simulated 0-10 cm soil water content from SiSPAT for both ecosystems with nevertheless a slight negative bias of -0.18 and -0.05 mm for the millet crop and the fallow respectively (Table C.2). For both ecosystems API is very well correlated to 0-10 cm soil water content with R^2 of 0.88 and 0.93 for the millet field and the fallow respectively (Table C.2). Likewise very good skill scores are obtained for soil evaporation for both ecosystems with again a slight negative bias supposed mainly due to API underestimation (Table C.2).

Table C.2. Skill scores of PAMEAS calibration over the 2005-2012 periods against SiSPAT (units of bias and RMSE are given with variable acronym, NSE and R^2 are dimensionless)

	Millet				Fallow			
	Bias	**RMSE**	**NSE**	**R^2**	**Bias**	**RMSE**	**NSE**	**R^2**
API (mm)	-0.18	0.85	0.88	0.88	-0.05	0.74	0.92	0.93
E (mm.day^{-1})	-0.07	0.43	0.83	0.84	-0.04	0.43	0.89	0.89
T (mm.day^{-1})	0.08	0.20	0.88	0.90	0.02	0.25	0.82	0.83
ET (mm.day^{-1})	-0.01	0.49	0.85	0.85	-0.03	0.50	0.90	0.90

For transpiration, PAMEAS is in good agreement with SiSPAT during the ascending phase of the transpiration cycle. During this period we observed an increase of the root zone soil moisture with an infiltration from the surface to deep layers, peaking at a maximum shortly after the last rainfall (not shown). During this period sensible heat (H) is relatively constant and near zero, all of the available energy at the surface is thus used for ET. Vegetation is not stressed and transpiration variations are mainly controlled by incoming solar radiation. Once this root zone soil moisture peak has passed, transpiration is capping, and supports all the ET since surface water content is dried up. H is increasing leading to a competition for available energy between *T* and the heating of the surface. Stomatal resistance term is more and more preponderant and vegetation is thus subject to water stress. Finally transpiration is rapidly decreasing less or more exponentially following the root zone soil water content depletion with very low sensitivity to incoming radiation. Consequently, as expected, during this phase PAMEAS is significantly less correlated with SiSPAT since it does not take into account any water stress (not shown). For purposes of application in a data fusion approach with MODIS-based E3S estimates this model's drift is not critical because images frequency is high during this period (Allies et al., 2020) and day to day ET variation are slight. Finally, adding *E* and *T* terms, ET simulated by PAMEAS is in very good agreement with SiSPAT with NSE values of 0.85 and 0.90 for the millet crop and the fallow respectively (Table C.2 and Figure C.1).

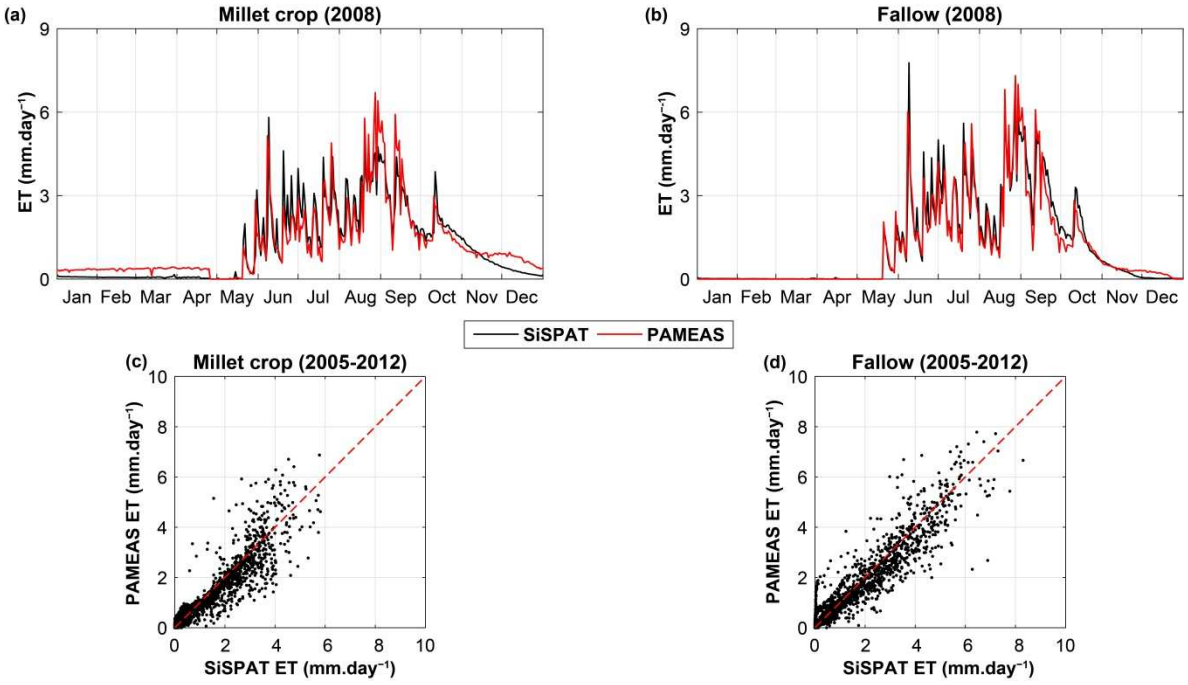

Figure C.1. Daily ET simulated by PAMEAS against ET simulated by SiSPAT for 2008 (top row panel) and 2005-2012 (bottom row panel) for the millet crop (a, c) and the fallow (b, d).

References

Albergel, C., Munier, S., Leroux, D., Dewaele, H., Fairbairn, D., Lavinia Barbu, A., Gelati, E., Dorigo, W., Faroux, S., Meurey, C., Le Moigne, P., Decharme, B., Mahfouf, J.-F., Calvet, J.-C., 2017. Sequential assimilation of satellite-derived vegetation and soil moisture products using SURFEX_v8.0: LDAS-Monde assessment over the Euro-Mediterranean area. Geosci. Model Dev. 10, 3889–3912. https://doi.org/10.5194/gmd-10-3889-2017

Alfieri, J.G., Anderson, M.C., Kustas, W.P., Cammalleri, C., 2017. Effect of the revisit interval and temporal upscaling methods on the accuracy of remotely sensed evapotranspiration estimates. Hydrol. Earth Syst. Sci. 21, 83–98. https://doi.org/10.5194/hess-21-83-2017

Alfieri, J.G., Blanken, P.D., Yates, D.N., Steffen, K., 2007. Variability in the Environmental Factors Driving Evapotranspiration from a Grazed Rangeland during Severe Drought Conditions. J. Hydrometeorol. 8, 207–220. https://doi.org/10.1175/JHM569.1

Allen, R.G., Pereira, L.S., Raes, D., Smith, M., 1998. Crop evapotranspiration - guidelines for computing crop water requirements (FAO irrigation and drainage paper No. 56). Rome (Italie).

Allies, A., Demarty, J., Olioso, A., Moussa, I.B., Issoufou, H.B.-A., Velluet, C., Bahir, M., Maïnassara, I., Oï, M., Chazarin, J.-P., Cappelaere, B., 2020. Evapotranspiration Estimation in the Sahel Using a New Ensemble-Contextual Method. Remote Sens. 12, 380. https://doi.org/10.3390/rs12030380

Anderson, M.C., Hain, C., Wardlow, B., Pimstein, A., Mecikalski, J.R., Kustas, W.P., 2010. Evaluation of Drought Indices Based on Thermal Remote Sensing of Evapotranspiration over the Continental United States. J. Clim. 24, 2025–2044. https://doi.org/10.1175/2010JCLI3812.1

Anderson, M.C., Zolin, C.A., Sentelhas, P.C., Hain, C.R., Semmens, K., Tugrul Yilmaz, M., Gao, F., Otkin, J.A., Tetrault, R., 2016. The Evaporative Stress Index as an indicator of agricultural drought in Brazil: An assessment based on crop yield impacts. Remote Sens. Environ. 174, 82–99. https://doi.org/10.1016/j.rse.2015.11.034

Balsamo, G., Pappenberger, F., Dutra, E., Viterbo, P., Hurk, B. van den, 2011. A revised land hydrology in the ECMWF model: a step towards daily water flux prediction in a fully-closed water cycle. Hydrol. Process. 25, 1046–1054. https://doi.org/10.1002/hyp.7808

Beck, H.E., van Dijk, A.I.J.M., Levizzani, V., Schellekens, J., Miralles, D.G., Martens, B., de Roo, A., 2017. MSWEP: 3-hourly 0.25° global gridded precipitation (1979–2015) by merging gauge, satellite, and reanalysis data. Hydrol. Earth Syst. Sci. 21, 589–615. https://doi.org/10.5194/hess-21-589-2017

Best, M.J., Pryor, M., Clark, D.B., Rooney, G.G., Essery, R.L.H., Ménard, C.B., Edwards, J.M., Hendry, M.A., Porson, A., Gedney, N., Mercado, L.M., Sitch, S., Blyth, E., Boucher, O., Cox, P.M., Grimmond, C.S.B., Harding, R.J., 2011. The Joint UK Land Environment Simulator (JULES), model description – Part 1: Energy and water fluxes. Geosci Model Dev 4, 677–699. https://doi.org/10.5194/gmd-4-677-2011

Bhattarai, N., Quackenbush, L.J., Dougherty, M., Marzen, L.J., 2015. A simple Landsat–MODIS fusion approach for monitoring seasonal evapotranspiration at 30 m spatial resolution. Int. J. Remote Sens. 36, 115–143. https://doi.org/10.1080/01431161.2014.990645

Boone, A., Getirana, A.C.V., Demarty, J., Cappelaere, B., Galle, S., Grippa, M., Lebel, T., Mougin, E., Peugeot, C., Vischel, T., 2009. The African Monsoon Multidisciplinary Analyses (AMMA) Land surface Model Intercomparison Project Phase 2 (ALMIP2). GEWEX News 19, 9–10.

992 Boulain, N., Cappelaere, B., Ramier, D., Issoufou, H.B.A., Halilou, O., Seghieri, J.,
993 Guillemin, F., Oï, M., Gignoux, J., Timouk, F., 2009a. Towards an understanding of
994 coupled physical and biological processes in the cultivated Sahel – 2. Vegetation and
995 carbon dynamics. J. Hydrol. 375, 190–203.
996 https://doi.org/10.1016/j.jhydrol.2008.11.045
997 Boulain, N., Cappelaere, B., Séguis, L., Favreau, G., Gignoux, J., 2009b. Water balance and
998 vegetation change in the Sahel: A case study at the watershed scale with an eco-
999 hydrological model. J. Arid Environ. 73, 1125–1135.
1000 https://doi.org/10.1016/j.jaridenv.2009.05.008
1001 Boussetta, S., Balsamo, G., Beljaars, A., Panareda, A.-A., Calvet, J.-C., Jacobs, C., Hurk, B.
1002 van den, Viterbo, P., Lafont, S., Dutra, E., Jarlan, L., Balzarolo, M., Papale, D., Werf,
1003 G. van der, 2013. Natural land carbon dioxide exchanges in the ECMWF integrated
1004 forecasting system: Implementation and offline validation. J. Geophys. Res.
1005 Atmospheres 118, 5923–5946. https://doi.org/10.1002/jgrd.50488
1006 Braud, I., Dantas-Antonino, A.C., Vauclin, M., Thony, J.L., Ruelle, P., 1995. A simple soil-
1007 plant-atmosphere transfer model (SiSPAT) development and field verification. J.
1008 Hydrol. 166, 213–250. https://doi.org/10.1016/0022-1694(94)05085-C
1009 Cammalleri, C., Anderson, M.C., Gao, F., Hain, C.R., Kustas, W.P., 2014. Mapping daily
1010 evapotranspiration at field scales over rainfed and irrigated agricultural areas using
1011 remote sensing data fusion. Agric. For. Meteorol. 186, 1–11.
1012 https://doi.org/10.1016/j.agrformet.2013.11.001
1013 Cammalleri, C., Anderson, M.C., Gao, F., Hain, C.R., Kustas, W.P., 2013. A data fusion
1014 approach for mapping daily evapotranspiration at field scale. Water Resour. Res. 49,
1015 4672–4686. https://doi.org/10.1002/wrcr.20349
1016 Cappelaere, B., Descroix, L., Lebel, T., Boulain, N., Ramier, D., Laurent, J.-P., Favreau, G.,
1017 Boubkraoui, S., Boucher, M., Bouzou Moussa, I., Chaffard, V., Hiernaux, P.,
1018 Issoufou, H.B.A., Le Breton, E., Mamadou, I., Nazoumou, Y., Oi, M., Ottlé, C.,
1019 Quantin, G., 2009. The AMMA-CATCH experiment in the cultivated Sahelian area of
1020 south-west Niger – Investigating water cycle response to a fluctuating climate and
1021 changing environment. J. Hydrol. 375, 34–51.
1022 https://doi.org/10.1016/j.jhydrol.2009.06.021
1023 Chen, M., Shi, W., Xie, P., Silva, V.B.S., Kousky, V.E., Higgins, R.W., Janowiak, J.E., 2008.
1024 Assessing objective techniques for gauge-based analyses of global daily precipitation.
1025 J. Geophys. Res. Atmospheres 113. https://doi.org/10.1029/2007JD009132
1026 Clark, D.B., Mercado, L.M., Sitch, S., Jones, C.D., Gedney, N., Best, M.J., Pryor, M.,
1027 Rooney, G.G., Essery, R.L.H., Blyth, E., Boucher, O., Harding, R.J., Huntingford, C.,
1028 Cox, P.M., 2011. The Joint UK Land Environment Simulator (JULES), model
1029 description – Part 2: Carbon fluxes and vegetation dynamics. Geosci Model Dev 4,
1030 701–722. https://doi.org/10.5194/gmd-4-701-2011
1031 d'Orgeval, T., Polcher, J., de Rosnay, P., 2008. Sensitivity of the West African hydrological
1032 cycle in ORCHIDEE to infiltration processes. Hydrol Earth Syst Sci 12, 1387–1401.
1033 https://doi.org/10.5194/hess-12-1387-2008
1034 Decharme, B., Ottlé, C., Saux-Picart, S., Boulain, N., Cappelaere, B., Ramier, D., Zribi, M.,
1035 2009. A New Land Surface Hydrology within the Noah-WRF Land-Atmosphere
1036 Mesoscale Model Applied to Semiarid Environment: Evaluation over the Dantiandou
1037 Kori (Niger). Adv. Meteorol. 1–13. http://dx.doi.org/10.1155/2009/731874
1038 Dee, D.P., Uppala, S.M., Simmons, A.J., Berrisford, P., Poli, P., Kobayashi, S., Andrae, U.,
1039 Balmaseda, M.A., Balsamo, G., Bauer, P., Bechtold, P., Beljaars, A.C.M., van de
1040 Berg, L., Bidlot, J., Bormann, N., Delsol, C., Dragani, R., Fuentes, M., Geer, A.J.,
1041 Haimberger, L., Healy, S.B., Hersbach, H., Hólm, E.V., Isaksen, L., Kållberg, P.,

Köhler, M., Matricardi, M., McNally, A.P., Monge-Sanz, B.M., Morcrette, J.-J., Park, B.-K., Peubey, C., de Rosnay, P., Tavolato, C., Thépaut, J.-N., Vitart, F., 2011. The ERA-Interim reanalysis: configuration and performance of the data assimilation system. Q. J. R. Meteorol. Soc. 137, 553–597. https://doi.org/10.1002/qj.828

Delogu, E., Olioso, A., Alliès, A., Demarty, J., Boulet, G., 2021. Evaluation of Multiple Methods for the Production of Continuous Evapotranspiration Estimates from TIR Remote Sensing. Remote Sens. 13, 1086. https://doi.org/10.3390/rs13061086

Eswar, R., Sekhar, M., Bhattacharya, B.K., 2016. Disaggregation of LST over India: comparative analysis of different vegetation indices. Int. J. Remote Sens. 37, 1035–1054. https://doi.org/10.1080/01431161.2016.1145363

Fisher, J.B., Melton, F., Middleton, E., Hain, C., Anderson, M., Allen, R., McCabe, M.F., Hook, S., Baldocchi, D., Townsend, P.A., Kilic, A., Tu, K., Miralles, D.D., Perret, J., Lagouarde, J.-P., Waliser, D., Purdy, A.J., French, A., Schimel, D., Famiglietti, J.S., Stephens, G., Wood, E.F., 2017. The future of evapotranspiration: Global requirements for ecosystem functioning, carbon and climate feedbacks, agricultural management, and water resources. Water Resour. Res. 53, 2618–2626. https://doi.org/10.1002/2016WR020175

Funk, C., Peterson, P., Landsfeld, M., Pedreros, D., Verdin, J., Shukla, S., Husak, G., Rowland, J., Harrison, L., Hoell, A., Michaelsen, J., 2015. The climate hazards infrared precipitation with stations—a new environmental record for monitoring extremes. Sci. Data 2, sdata201566. https://doi.org/10.1038/sdata.2015.66

Galle, S., Grippa, M., Peugeot, C., Moussa, I.B., Cappelaere, B., Demarty, J., Mougin, E., Panthou, G., Adjomayi, P., Agbossou, E.K., Ba, A., Boucher, M., Cohard, J.-M., Descloitres, M., Descroix, L., Diawara, M., Dossou, M., Favreau, G., Gangneron, F., Gosset, M., Hector, B., Hiernaux, P., Issoufou, B.-A., Kergoat, L., Lawin, E., Lebel, T., Legchenko, A., Abdou, M.M., Malam-Issa, O., Mamadou, O., Nazoumou, Y., Pellarin, T., Quantin, G., Sambou, B., Seghieri, J., Séguis, L., Vandervaere, J.-P., Vischel, T., Vouillamoz, J.-M., Zannou, A., Afouda, S., Alhassane, A., Arjounin, M., Barral, H., Biron, R., Cazenave, F., Chaffard, V., Chazarin, J.-P., Guyard, H., Koné, A., Mainassara, I., Mamane, A., Oi, M., Ouani, T., Soumaguel, N., Wubda, M., Ago, E.E., Alle, I.C., Allies, A., Arpin-Pont, F., Awessou, B., Cassé, C., Charvet, G., Dardel, C., Depeyre, A., Diallo, F.B., Do, T., Fatras, C., Frappart, F., Gal, L., Gascon, T., Gibon, F., Guiro, I., Ingatan, A., Kempf, J., Kotchoni, D.O.V., Lawson, F.M.A., Leauthaud, C., Louvet, S., Mason, E., Nguyen, C.C., Perrimond, B., Pierre, C., Richard, A., Robert, E., Román-Cascón, C., Velluet, C., Wilcox, C., 2018. AMMA-CATCH, a Critical Zone Observatory in West Africa Monitoring a Region in Transition. Vadose Zone J. 17. https://doi.org/10.2136/vzj2018.03.0062

Gallego-Elvira, B., Olioso, A., Mira, M., Castillo, S.R.-, Boulet, G., Marloie, O., Garrigues, S., Courault, D., Weiss, M., Chauvelon, P., Boutron, O., 2013. EVASPA (EVapotranspiration Assessment from SPAce) Tool: An overview. Procedia Environ. Sci. 19, 303–310. https://doi.org/10.1016/j.proenv.2013.06.035

Gao, F., Masek, J., Schwaller, M., Hall, F., 2006. On the blending of the Landsat and MODIS surface reflectance: predicting daily Landsat surface reflectance. IEEE Trans. Geosci. Remote Sens. 44, 2207–2218. https://doi.org/10.1109/TGRS.2006.872081

Gevaert, C.M., García-Haro, F.J., 2015. A comparison of STARFM and an unmixing-based algorithm for Landsat and MODIS data fusion. Remote Sens. Environ. 156, 34–44. https://doi.org/10.1016/j.rse.2014.09.012

Grippa, M., Kergoat, L., Boone, A., Peugeot, C., Demarty, J., Cappelaere, B., Gal, L., Hiernaux, P., Mougin, E., Ducharne, A., Dutra, E., Anderson, M., Hain, C., 2017. Modelling surface runoff and water fluxes over contrasted soils in pastoral Sahel:

evaluation of the ALMIP2 land surface models over the Gourma region in Mali. J. Hydrometeorol. https://doi.org/10.1175/JHM-D-16-0170.1
Guillevic, P.C., Olioso, A., Hook, S.J., Fisher, J.B., Lagouarde, J.-P., Vermote, E.F., 2019. Impact of the Revisit of Thermal Infrared Remote Sensing Observations on Evapotranspiration Uncertainty—A Sensitivity Study Using AmeriFlux Data. Remote Sens. 11, 573. https://doi.org/10.3390/rs11050573
Huffman, G.J., Bolvin, D.T., Nelkin, E.J., Wolff, D.B., Adler, R.F., Gu, G., Hong, Y., Bowman, K.P., Stocker, E.F., 2007. The TRMM Multisatellite Precipitation Analysis (TMPA): Quasi-Global, Multiyear, Combined-Sensor Precipitation Estimates at Fine Scales. J. Hydrometeorol. 8, 38–55. https://doi.org/10.1175/JHM560.1
Joseph, R., Smith, T.M., Sapiano, M.R.P., Ferraro, R.R., 2009. A New High-Resolution Satellite-Derived Precipitation Dataset for Climate Studies. J. Hydrometeorol. 10, 935–952. https://doi.org/10.1175/2009JHM1096.1
Joyce, R.J., Janowiak, J.E., Arkin, P.A., Xie, P., 2004. CMORPH: A Method that Produces Global Precipitation Estimates from Passive Microwave and Infrared Data at High Spatial and Temporal Resolution. J. Hydrometeorol. 5, 487–503. https://doi.org/10.1175/1525-7541(2004)005<0487:CAMTPG>2.0.CO;2
Jung, M., Reichstein, M., Ciais, P., Seneviratne, S.I., Sheffield, J., Goulden, M.L., Bonan, G., Cescatti, A., Chen, J., de Jeu, R., Dolman, A.J., Eugster, W., Gerten, D., Gianelle, D., Gobron, N., Heinke, J., Kimball, J., Law, B.E., Montagnani, L., Mu, Q., Mueller, B., Oleson, K., Papale, D., Richardson, A.D., Roupsard, O., Running, S., Tomelleri, E., Viovy, N., Weber, U., Williams, C., Wood, E., Zaehle, S., Zhang, K., 2010. Recent decline in the global land evapotranspiration trend due to limited moisture supply. Nature 467, 951–954. https://doi.org/10.1038/nature09396
Kalma, J.D., McVicar, T.R., McCabe, M.F., 2008. Estimating Land Surface Evaporation: A Review of Methods Using Remotely Sensed Surface Temperature Data. Surv. Geophys. 29, 421–469. https://doi.org/10.1007/s10712-008-9037-z
Kaptué Tchuenté, A.T., Roujean, J.-L., De Jong, S.M., 2011. Comparison and relative quality assessment of the GLC2000, GLOBCOVER, MODIS and ECOCLIMAP land cover data sets at the African continental scale. Int. J. Appl. Earth Obs. Geoinformation 13, 207–219. https://doi.org/10.1016/j.jag.2010.11.005
Katul, G.G., Oren, R., Manzoni, S., Higgins, C., Parlange, M.B., 2012. Evapotranspiration: A process driving mass transport and energy exchange in the soil-plant-atmosphere-climate system. Rev. Geophys. 50, RG3002. https://doi.org/10.1029/2011RG000366
Ke, Y., Im, J., Park, S., Gong, H., 2017. Spatiotemporal downscaling approaches for monitoring 8-day 30m actual evapotranspiration. ISPRS J. Photogramm. Remote Sens. 126, 79–93. https://doi.org/10.1016/j.isprsjprs.2017.02.006
Kohler, M.A., Linsley, R.K., 1951. Predicting the Runoff from Storm Rainfall. U.S. Department of Commerce, Weather Bureau.
Koster, R.D., Suarez, M.J., 1992. Modeling the land surface boundary in climate models as a composite of independent vegetation stands - Koster - 1992 - Journal of Geophysical Research: Atmospheres - Wiley Online Library. J. Geophys. Res. Atmospheres 97, 2697–2715. https://doi.org/10.1029/91JD01696
Koster, R.D., Suarez, M.J., Ducharne, A., Stieglitz, M., Kumar, P., 2000. A catchment-based approach to modeling land surface processes in a general circulation model: 1. Model structure - Koster - 2000 - Journal of Geophysical Research: Atmospheres - Wiley Online Library. J. Geophys. Res. Atmospheres 105, 24,809-822. https://doi.org/10.1029/2000JD900327
Kunnath-Poovakka, A., Ryu, D., Renzullo, L.J., George, B., 2016. The efficacy of calibrating hydrologic model using remotely sensed evapotranspiration and soil moisture for

streamflow prediction. J. Hydrol. 535, 509–524. https://doi.org/10.1016/j.jhydrol.2016.02.018
Lagouarde, J.-P., Bach, M., Sobrino, J.A., Boulet, G., Briottet, X., Cherchali, S., Coudert, B., Dadou, I., Dedieu, G., Gamet, P., Hagolle, O., Jacob, F., Nerry, F., Olioso, A., Ottlé, C., Roujean, J., Fargant, G., 2013. The MISTIGRI thermal infrared project: scientific objectives and mission specifications. Int. J. Remote Sens. 34, 3437–3466. https://doi.org/10.1080/01431161.2012.716921
Lagouarde, J.-P., Olioso, A., Roujean, J.-L., Boulet, G., Coudert, B., Dayau, S., Castillo, S., Weiss, M., 2010. Defining the revisit frequency for the MISTIGRI project of a satellite mission in the thermal infrared, in: International Symposium on Recent Advances in Quantitative Remote Sensing: RAQRS'III. Torrent, Valencia, Espagne, pp. 824–829.
Lawrence, D.M., Oleson, K.W., Flanner, M.G., Thornton, P.E., Swenson, S.C., Lawrence, P.J., Zeng, X., Yang, Z.-L., Levis, S., Sakaguchi, K., Bonan, G.B., Slater, A.G., 2011. Parameterization improvements and functional and structural advances in Version 4 of the Community Land Model. J. Adv. Model. Earth Syst. 3. https://doi.org/10.1029/2011MS00045
Leblanc, M.J., Favreau, G., Massuel, S., Tweed, S.O., Loireau, M., Cappelaere, B., 2008. Land clearance and hydrological change in the Sahel: SW Niger. Glob. Planet. Change 61, 135–150. https://doi.org/10.1016/j.gloplacha.2007.08.011
Leduc, C., Bromley, J., Schroeter, P., 1997. Water table fluctuation and recharge in semi-arid climate: some results of the HAPEX-Sahel hydrodynamic survey (Niger). J. Hydrol., HAPEX-Sahel 188–189, 123–138. https://doi.org/10.1016/S0022-1694(96)03156-3
Li, W., Baret, F., Weiss, M., Buis, S., Lacaze, R., Demarez, V., Dejoux, J., Battude, M., Camacho, F., 2017. Combining hectometric and decametric satellite observations to provide near real time decametric FAPAR product. Remote Sens. Environ. 200, 250–262. https://doi.org/10.1016/j.rse.2017.08.018
Liu, Y.Y., Dorigo, W.A., Parinussa, R.M., de Jeu, R.A.M., Wagner, W., McCabe, M.F., Evans, J.P., van Dijk, A.I.J.M., 2012. Trend-preserving blending of passive and active microwave soil moisture retrievals. Remote Sens. Environ. 123, 280–297. https://doi.org/10.1016/j.rse.2012.03.014
Lohou, F., Kergoat, L., Guichard, F., Boone, A., Cappelaere, B., Cohard, J.-M., Demarty, J., Galle, S., Grippa, M., Peugeot, C., Ramier, D., Taylor, C.M., Timouk, F., 2014. Surface response to rain events throughout the West African monsoon. Atmospheric Chem. Phys. 14, 3883–3898. https://doi.org/10.5194/acp-14-3883-2014
Ma, Y., Liu, S., Song, L., Xu, Z., Liu, Y., Xu, T., Zhu, Z., 2018. Estimation of daily evapotranspiration and irrigation water efficiency at a Landsat-like scale for an arid irrigation area using multi-source remote sensing data. Remote Sens. Environ. 216, 715–734. https://doi.org/10.1016/j.rse.2018.07.019
Marshall, M., Funk, C., Michaelsen, J., 2012. Examining evapotranspiration trends in Africa. Clim. Dyn. 38, 1849–1865. https://doi.org/10.1007/s00382-012-1299-y
Marshall, M., Tu, K., Funk, C., Michaelsen, J., Williams, P., Williams, C., Ardö, J., Boucher, M., Cappelaere, B., de Grandcourt, A., Nickless, A., Nouvellon, Y., Scholes, R., Kutsch, W., 2013. Improving operational land surface model canopy evapotranspiration in Africa using a direct remote sensing approach. Hydrol. Earth Syst. Sci. 17, 1079–1091. https://doi.org/10.5194/hess-17-1079-2013
Martens, B., Miralles, D.G., Lievens, H., van der Schalie, R., de Jeu, R.A.M., Fernández-Prieto, D., Beck, H.E., Dorigo, W.A., Verhoest, N.E.C., 2017. GLEAM v3: satellite-based land evaporation and root-zone soil moisture. Geosci. Model Dev. 10, 1903–1925. https://doi.org/10.5194/gmd-10-1903-2017

Mauder, M., Foken, T., 2004. Documentation and instruction manual of the eddy covariance software package TK2 (U. Bayreuth, Abt. Mikrometeorologie, Bayreuth, Germany).

Merlin, O., Al Bitar, A., Rivalland, V., Béziat, P., Ceschia, E., Dedieu, G., 2010. An Analytical Model of Evaporation Efficiency for Unsaturated Soil Surfaces with an Arbitrary Thickness. J. Appl. Meteorol. Climatol. 50, 457–471. https://doi.org/10.1175/2010JAMC2418.1

Merlin, O., Stefan, V.G., Amazirh, A., Chanzy, A., Ceschia, E., Er-Raki, S., Gentine, P., Tallec, T., Ezzahar, J., Bircher, S., Beringer, J., Khabba, S., 2016. Modeling soil evaporation efficiency in a range of soil and atmospheric conditions using a meta-analysis approach. Water Resour. Res. 52, 3663–3684. https://doi.org/10.1002/2015WR018233

Miralles, D.G., Holmes, T.R.H., De Jeu, R.A.M., Gash, J.H., Meesters, A.G.C.A., Dolman, A.J., 2011. Global land-surface evaporation estimated from satellite-based observations. Hydrol. Earth Syst. Sci. 15, 453–469. https://doi.org/10.5194/hess-15-453-2011

Nasonova, O.N., Gusev, E.M., Ayzel, G.V., 2015. Optimizing land surface parameters for simulating river runoff from 323 MOPEX-watersheds. Water Resour. 42, 186–197. https://doi.org/10.1134/S0097807815020104

Noilhan, J., Mahfouf, J.-F., 1996. The ISBA land surface parameterisation scheme. Glob. Planet. Change, Soil Moisture Simulation 13, 145–159. https://doi.org/10.1016/0921-8181(95)00043-7

Olioso, A., Allies, A., Boulet, G., Delogu, E., Demarty, J., Gallego-Elvira, B., Marloie, O., Chauvelon, P., Boutron, O., Buis, S., Weiss, M., Velluet, C., Bahir, M., 2018. Monitoring evapotranspiration with remote sensing data and ground data using ensemble model averaging, in: International Geoscience and Remote Sensing Symposium, IGARSS '18. IEE, Valencia, Spain.

Olioso, A., Bahir, M., Gallego-Elvira, B., Garrigues, S., Mira, M., Chanzy, A., Weiss, M., Marloie, O., Boulet, G., 2015. Monitoring evapotranspiration over the Crau Aquifer from remote sensing and flux tower data., in: International Conference MISTRALS "Environment in the Mediterranean Statements and Prospects for Research and Society." Marseille, France.

Olioso, A., Ollivier, C., Martin, N., Simioni, G., Weiss, M., Guillevic, P.C., Marloie, O., Carriere, S., Davi, H., Huard, F., 2019. Monitoring Vegetation Fraction Cover of French Mediterranean Forests for Evapotranspiration and Water Stress Mapping, in: ESA Living Planet Symposium 2019. Milan, Italy.

Olivera-Guerra, L., Mattar, C., Merlin, O., Durán-Alarcón, C., Santamaría-Artigas, A., Fuster, R., 2017. An operational method for the disaggregation of land surface temperature to estimate actual evapotranspiration in the arid region of Chile. ISPRS J. Photogramm. Remote Sens. 128, 170–181. https://doi.org/10.1016/j.isprsjprs.2017.03.014

Ollivier, C., Olioso, A., Carrière, S.D., Boulet, G., Chalikakis, K., Chanzy, A., Charlier, J.-B., Combemale, D., Davi, H., Emblanch, C., Marloie, O., Martin-StPaul, N., Mazzilli, N., Simioni, G., Weiss, M., 2021. An evapotranspiration model driven by remote sensing data for assessing groundwater resource in karst watershed. Sci. Total Environ. 781, 146706. https://doi.org/10.1016/j.scitotenv.2021.146706

Otkin, J.A., Anderson, M.C., Hain, C., Svoboda, M., Johnson, D., Mueller, R., Tadesse, T., Wardlow, B., Brown, J., 2016. Assessing the evolution of soil moisture and vegetation conditions during the 2012 United States flash drought. Agric. For. Meteorol. 218–219, 230–242. https://doi.org/10.1016/j.agrformet.2015.12.065

Pierre, C., Grippa, M., Mougin, E., Guichard, F., Kergoat, L., 2016. Changes in Sahelian annual vegetation growth and phenology since 1960: A modeling approach. Glob. Planet. Change 143, 162–174. https://doi.org/10.1016/j.gloplacha.2016.06.009

Ramier, D., Boulain, N., Cappelaere, B., Timouk, F., Rabanit, M., Lloyd, C.R., Boubkraoui, S., Métayer, F., Descroix, L., Wawrzyniak, V., 2009. Towards an understanding of coupled physical and biological processes in the cultivated Sahel – 1. Energy and water. J. Hydrol. 375, 204–216. https://doi.org/10.1016/j.jhydrol.2008.12.002

Roerink, G.J., Su, Z., Menenti, M., 2000. S-SEBI: A simple remote sensing algorithm to estimate the surface energy balance. Phys. Chem. Earth Part B Hydrol. Oceans Atmosphere 25, 147–157. https://doi.org/10.1016/S1464-1909(99)00128-8

Ruggieri, G., Allocca, V., Borfecchia, F., Cusano, D., Marsiglia, P., De Vita, P., 2021. Testing Evapotranspiration Estimates Based on MODIS Satellite Data in the Assessment of the Groundwater Recharge of Karst Aquifers in Southern Italy. Water 13, 118. https://doi.org/10.3390/w13020118

Ryu, Y., Baldocchi, D.D., Black, T.A., Detto, M., Law, B.E., Leuning, R., Miyata, A., Reichstein, M., Vargas, R., Ammann, C., Beringer, J., Flanagan, L.B., Gu, L., Hutley, L.B., Kim, J., McCaughey, H., Moors, E.J., Rambal, S., Vesala, T., 2012. On the temporal upscaling of evapotranspiration from instantaneous remote sensing measurements to 8-day mean daily-sums. Agric. For. Meteorol. 152, 212–222. https://doi.org/10.1016/j.agrformet.2011.09.010

Saha, S., Moorthi, S., Pan, H.-L., Wu, X., Wang, Jiande, Nadiga, S., Tripp, P., Kistler, R., Woollen, J., Behringer, D., Liu, H., Stokes, D., Grumbine, R., Gayno, G., Wang, Jun, Hou, Y.-T., Chuang, H., Juang, H.-M.H., Sela, J., Iredell, M., Treadon, R., Kleist, D., Van Delst, P., Keyser, D., Derber, J., Ek, M., Meng, J., Wei, H., Yang, R., Lord, S., van den Dool, H., Kumar, A., Wang, W., Long, C., Chelliah, M., Xue, Y., Huang, B., Schemm, J.-K., Ebisuzaki, W., Lin, R., Xie, P., Chen, M., Zhou, S., Higgins, W., Zou, C.-Z., Liu, Q., Chen, Y., Han, Y., Cucurull, L., Reynolds, R.W., Rutledge, G., Goldberg, M., 2010. The NCEP Climate Forecast System Reanalysis. Bull. Am. Meteorol. Soc. 91, 1015–1058. https://doi.org/10.1175/2010BAMS3001.1

Santos, C., Lorite, I.J., Tasumi, M., Allen, R.G., Fereres, E., 2007. Integrating satellite-based evapotranspiration with simulation models for irrigation management at the scheme level. Irrig. Sci. 26, 277–288. https://doi.org/10.1007/s00271-007-0093-9

Saux-Picart, S., Ottlé, C., Perrier, A., Decharme, B., Coudert, B., Zribi, M., Boulain, N., Cappelaere, B., Ramier, D., 2009. SEtHyS_Savannah: A multiple source land surface model applied to Sahelian landscapes. Agric. For. Meteorol. 149, 1421–1432. https://doi.org/10.1016/j.agrformet.2009.03.013

Saxton, K.E., Rawls, W.J., Romberger, J.S., Papendick, R.I., 1986. Estimating Generalized Soil-water Characteristics from Texture. Soil Sci. Soc. Am. J. 50, 1031–1036. https://doi.org/10.2136/sssaj1986.03615995005000040039x

Schneider, U., Becker, A., Finger, P., Meyer-Christoffer, A., Ziese, M., Rudolf, B., 2014. GPCC's new land surface precipitation climatology based on quality-controlled in situ data and its role in quantifying the global water cycle. Theor. Appl. Climatol. 115, 15–40. https://doi.org/10.1007/s00704-013-0860-x

Schuurmans, J.M., Troch, P.A., Veldhuizen, A.A., Bastiaanssen, W.G.M., Bierkens, M.F.P., 2003. Assimilation of remotely sensed latent heat flux in a distributed hydrological model. Adv. Water Resour. 26, 151–159. https://doi.org/10.1016/S0309-1708(02)00089-1

Semmens, K.A., Anderson, M.C., Kustas, W.P., Gao, F., Alfieri, J.G., McKee, L., Prueger, J.H., Hain, C.R., Cammalleri, C., Yang, Y., Xia, T., Sanchez, L., Mar Alsina, M., Vélez, M., 2016. Monitoring daily evapotranspiration over two California vineyards

using Landsat 8 in a multi-sensor data fusion approach. Remote Sens. Environ., Landsat 8 Science Results 185, 155–170. https://doi.org/10.1016/j.rse.2015.10.025
Shmakin, A.B., 1998. The updated version of SPONSOR land surface scheme: PILPS-influenced improvements. Glob. Planet. Change 19, 49–62. https://doi.org/10.1016/S0921-8181(98)00041-1
Sjöström, M., Zhao, M., Archibald, S., Arneth, A., Cappelaere, B., Falk, U., de Grandcourt, A., Hanan, N., Kergoat, L., Kutsch, W., Merbold, L., Mougin, E., Nickless, A., Nouvellon, Y., Scholes, R.J., Veenendaal, E.M., Ardö, J., 2013. Evaluation of MODIS gross primary productivity for Africa using eddy covariance data. Remote Sens. Environ. 131, 275–286. https://doi.org/10.1016/j.rse.2012.12.023
Takata, K., Emori, S., Watanabe, T., 2003. Development of the minimal advanced treatments of surface interaction and runoff. Glob. Planet. Change, Project for Intercomparison of Land-surface Parameterization Schemes, Phase 2(e) 38, 209–222. https://doi.org/10.1016/S0921-8181(03)00030-4
Tobin, K.J., Bennett, M.E., 2017. Constraining SWAT Calibration with Remotely Sensed Evapotranspiration Data. JAWRA J. Am. Water Resour. Assoc. 53, 593–604. https://doi.org/10.1111/1752-1688.12516
Toureiro, C., Serralheiro, R., Shahidian, S., Sousa, A., 2017. Irrigation management with remote sensing: Evaluating irrigation requirement for maize under Mediterranean climate condition. Agric. Water Manag. 184, 211–220. https://doi.org/10.1016/j.agwat.2016.02.010
Trigo, I.F., Dacamara, C.C., Viterbo, P., Roujean, J.-L., Olesen, F., Barroso, C., Camacho-de-Coca, F., Carrer, D., Freitas, S.C., García-Haro, J., Geiger, B., Gellens-Meulenberghs, F., Ghilain, N., Meliá, J., Pessanha, L., Siljamo, N., Arboleda, A., 2011. The Satellite Application Facility for Land Surface Analysis. Int. J. Remote Sens. 32, 2725–2744. https://doi.org/10.1080/01431161003743199
Velluet, C., 2014. Modélisation et analyse pluriannuelles du fonctionnement hydrologique et énergétique de deux écosystèmes dominants au Sahel agropastoral (Sud-Ouest Niger) (Thèse de Doctorat). Université Montpellier II - Sciences et Techniques du Languedoc, Montpellier, France.
Velluet, C., Demarty, J., Cappelaere, B., Braud, I., Issoufou, H.B.A., Boulain, N., Ramier, D., Mainassara, I., Charvet, G., Boucher, M., Chazarin, J.P., Oï, M., Yahou, H., Maidaji, B., Pont, F.A., Benarrosh, N., Mahamane, A., Nazoumou, Y., Favreau, G., Seghieri, J., 2014. Building a field- and model-based climatology of surface energy and water cycles for dominant land cover types in the cultivated Sahel. Annual budgets and seasonality. Hydrol. Earth Syst. Sci. 18, 5001–5024. https://doi.org/10.5194/hess-18-5001-2014
Verseghy, D.L., 1991. Class—A Canadian land surface scheme for GCMS. I. Soil model. Int. J. Climatol. 11, 111–133. https://doi.org/10.1002/joc.3370110202
Vischel, T., Quantin, G., Lebel, T., Viarre, J., Gosset, M., Cazenave, F., Panthou, G., 2011. Generation of High-Resolution Rain Fields in West Africa: Evaluation of Dynamic Interpolation Methods. J. Hydrometeorol. 12, 1465–1482. https://doi.org/10.1175/JHM-D-10-05015.1
Wagner, W., Dorigo, W., de Jeu, R., Fernandez, D., Benveniste, J., Haas, E., Ertl, M., 2012. Fusion of Active and Passive Microwave Observations to Create AN Essential Climate Variable Data Record on Soil Moisture. ISPRS Ann. Photogramm. Remote Sens. Spat. Inf. Sci. 7, 315–321. https://doi.org/10.5194/isprsannals-I-7-315-2012
Wang, P., Gao, F., Masek, J.G., 2014. Operational Data Fusion Framework for Building Frequent Landsat-Like Imagery. IEEE Trans. Geosci. Remote Sens. 52, 7353–7365. https://doi.org/10.1109/TGRS.2014.2311445

Xu, C.-Y., Singh, V.P., 2000. Evaluation and generalization of radiation-based methods for calculating evaporation. Hydrol. Process. 14, 339–349. https://doi.org/10.1002/(SICI)1099-1085(20000215)14:2<339::AID-HYP928>3.0.CO;2-O

Zhang, C., Long, D., Zhang, Y., Anderson, M.C., Kustas, W.P., Yang, Y., 2021. A decadal (2008–2017) daily evapotranspiration data set of 1 km spatial resolution and spatial completeness across the North China Plain using TSEB and data fusion. Remote Sens. Environ. 262, 112519. https://doi.org/10.1016/j.rse.2021.112519

Zhang, K., Kimball, J.S., Running, S.W., 2016. A review of remote sensing based actual evapotranspiration estimation. Wiley Interdiscip. Rev. Water 3, 834–853. https://doi.org/10.1002/wat2.1168